From micro to macroevolution: drivers of shape variation in an island radiation of *Podarcis* lizards

Abstract

Phenotypic traits have been shown to evolve in response to variation in the environment. However, the evolutionary processes underlying the emergence of phenotypic diversity can typically only be understood at the population level. Consequently, how subtle phenotypic differences at the intraspecific level can give rise to larger-scale changes in performance and ecology remains poorly understood. We here tested for the covariation between ecology, bite force, jaw muscle architecture, and the three-dimensional shape of the cranium and mandible in 16 insular populations of the lizards *Podarcis melisellensis* and *P. sicula*. We then compared the patterns observed at the among-population level with those observed at the interspecific level. We found that three-dimensional head shape as well as jaw musculature evolve similarly under similar ecological circumstances. Depending on the type of food consumed or on the level of sexual competition, different muscle groups were more developed and appeared to underlie changes in cranium and mandible shape. Our findings show that the local selective regimes are primary drivers of phenotypic variation resulting in predictable patterns of form and function. Moreover, intraspecific patterns of variation were generally consistent with those at the interspecific level, suggesting that microevolutionary variation may translate into macroevolutionary patterns of ecomorphological diversity.

Keywords: bite force, diet, geometric morphometrics, head shape, intraspecific variation, island, lizards, sexual competition.

Introduction

Any biological structure is the result of the interplay between the phylogenetic heritage of the organism, its function, and its development (D'Arcy Thompson, 1942; Gould & Lewontin, 1979; Goodwin & Trainor, 1980; Pigliucci & Kaplan, 2000). The morphology of an organism thus reflects the constraints imposed by the physical and biological characteristics of its environment (Sagnes et al. 1997; Fish, 1998; Fish et al. 2008; Segall et al. 2019; Hedenström, 2002; Altshuler et al. 2015; Hedenström & Johansson, 2015) within the limits imposed by its genetic and developmental repertoire. Comparative studies have convincingly demonstrated that the evolution of phenotypic diversity occurs in response to the selective pressures imposed by different ecological contexts (e.g., Boag & Grant, 1981; Losos, 1990) or life-history strategies (Fabre et al. 2020, 2021). However, functional and constructional trade-offs may limit or constrain the expression of a given phenotype (Cheverud, 1982; Barel et al. 1989; Herrel et al. 2009). Moreover, genetic architecture may drive the direction and magnitude of phenotypic change (Lande, 1976), thus driving the evolution of traits along genetic lines of least resistance (Schluter, 1996, 2000; McGlothlin et al. 2018). This concept has been extended to phenotypic traits (Marroig & Cheverud, 2005; Renaud et al. 2011) suggesting that variation within and between populations is often aligned with selection acting on axes of variation most prominent within populations. Population-level studies are consequently particularly insightful in helping to understand the drivers of phenotypic variation because they can inform us on the processes driving variation in morphology (Stuart et al. 2014; Campbell-Staton et al. 2017; Donihue et al. 2018).

The skull has been studied extensively as it fulfills many essential tasks including feeding, the protection of the sensory organs and the brain, interactions with conspecifics or other species, and even locomotion in some taxa (Wake, 2003; Herrel et al. 2007). Consequently, the skull of vertebrates likely evolves in response to a variety of factors including physical constraints (Segall et al. 2020; Roscito & Rodrigues, 2010; Rodrigues et al. 2015; Da Silva et al. 2018), activity patterns (Martin & Ross, 2005), and foraging strategies (Reilly, Miles & McBrayer, 2007). However, complex integrated systems such as the vertebrate feeding system are not mechanically optimized structures (Zweers, 1979; Wake & Roth, 1989), rendering inferences of function from form often difficult and complex. The skull is composed of multiple bones arranged to carry out the aforementioned functions, while providing attachment areas for the masticatory muscles, and resisting the external forces generated during a behavior. As bone is a living tissue that is remodeled by the magnitude and the direction of the forces it experiences (Currey, 2002; Renaud et al. 2010), it can be expected that the shape of cranium and mandible are strongly integrated with jaw muscle architecture (Fabre et al. 2014a; Cornette et al. 2015; Fabre et al. 2018), masticatory function, and by inference, with the diet

of an animal. For these reasons, cranial shape can be expected to diverge quickly among populations that differ in local selective regimes. The skull thus represents a biological structure that is relevant to address questions on how microevolutionary processes drive changes in morphology which subsequently may translate into macroevolutionary patterns of phenotypic variation. Islands represent excellent study systems to address these questions as they are relatively simple and replicated ecosystems, allowing the drivers of variation in form and function to be teased apart (Losos, 2009; Losos & Ricklefs, 2009; Kueffer, Drake & Fernandez-Palacios, 2014). Moreover, insular systems often impose strong ecological pressures, thus favoring the emergence of adaptive responses in morphology (Baeckens & Van Damme, 2020).

A previous study (Taverne et al. 2019) highlighted natural variation in the diet and the ecology of insular populations of *Podarcis* lizards living on small islands in the Adriatic. These populations range from insectivorous to omnivorous, with lizards relying on difficult to chew food items (i.e., plant material and hard prey) to face the food scarcity observed in the smallest and most depauperate environments. Additionally, a recent study demonstrated that the proportion of these mechanically resistant items in the diet as well as the level of sexual competition are important drivers of variation in bite force in these lizards (Taverne et al. 2020). Variation in bite force is partly driven by variation in head shape (Herrel et al. 2001, 2010; Verwaijen et al. 2002; Lappin et al. 2006; Huyghe et al. 2009; Wittorski et al. 2016), as taller and wider heads provide more space for muscles (Herrel et al. 2007). However, relatively weak correlations between bite force and external head dimensions were detected in these insular *Podarcis* lizards (Taverne et al. 2020), suggesting that variation in bite force is probably driven more by variation in muscle architecture. Subtle morphological differences between populations underlying variation in muscle architecture are, however, likely not quantifiable through external and linear measurements (Lappin & Husak, 2005; Fabre et al. 2014b). Three-dimensional geometric morphometrics (Bookstein, 1997; Klingenberg, 2002, 2011; Gunz et al. 2005; Kaliontzopoulou, 2011; Adams, 2013) represents a powerful alternative for quantifying morphological variation, and determining how it relates to variation in performance and diet. Despite the availability of this tool, surprisingly few studies have quantified intraspecific morphological variation in skull shape in association with variation in muscles and bite force (but see Herrel et al. 2007; Fabre et al. 2014a).

The Croatian archipelago of the Adriatic is the second largest archipelago in the Mediterranean, comprising almost 700 islands and islets. This archipelago provides a unique opportunity to study independent populations of two species of *Podarcis* lizards, *Podarcis melisellensis* and *Podarcis sicula*. The islands in this archipelago were separated at the end of the last glaciation (approximately 18,000 years ago), when sea levels rose. Given the presence of both species on multiple islands, this system

permits us to explore whether intraspecific ecomorphological patterns are repeated at the interspecific level. To tackle this question, we carried out a comparative study including 139 specimens from 16 insular populations of the two *Podarcis* species. We first asked ourselves whether patterns of evolution in cranial morphology and anatomy occurring among populations are similar in similar ecological contexts. To do so, we used geometric morphometrics to test for the covariation between the shape of the skull and mandible in 3D, jaw musculature, bite force, and ecological variables.

We predict that variation in bite force and jaw musculature will co-vary with the type of food items consumed and with the level of sexual competition within the populations; that skull and mandible shape will covary with muscle architecture and with ecological traits. We predict that these patterns would hold even when accounting for the phylogenetic relationships between populations, suggesting that the masticatory apparatus is independently evolving towards similar morphologies under comparable ecological circumstances. Additionally, we predict that the evolutionary trajectories within each species will be congruent with those among species. Specifically, we predict that the functional associations of the skull and diet will be similar irrespective of the species considered.

Material and Methods

Specimens, ecological, and bite force data

The 16 populations of interest were sampled across 14 islands in the Adriatic and two mainland sites. Adult lizards were captured by noose or by hand at the end of the summer of 2016. In total, 455 specimens were captured (Table S1). All individuals were stomach-flushed right after capture using a syringe with ball-tipped steel needle (Herrel et al. 2006). Stomach contents were preserved in individual vials containing a 70% aqueous ethanol solution and analyzed as described in Taverne et al (2019). Briefly, we recorded the volumetric proportion of plants and hard arthropods consumed relative to the total volume of the bolus. Sexual dimorphism in head dimensions of each population was calculated. To do so, we measured head dimensions of every specimen, $\log_{10}$-transformed them, and calculated the mean distance between males and females along the first axes of a PCA. This measure of sexual dimorphism in head dimensions was previously demonstrated to be a good indicator for the level of sexual competition in these populations (Taverne et al. 2020). *In vivo* bite force was measured for all individuals as described in Taverne et al. (2020). To do so, we made lizards bite on the plates of a bite force set-up containing an isometric Kistler force transducer (type 9203) connected to a Kistler charge amplifier (type 5995, Kistler Inc., Winterthur, Switzerland; see Herrel et al. 1999 for a detailed description of the set-up) while standardizing gape and bite point.

CT scanning

We sacrificed five male and five female lizards of each population, where authorized (see Table S1), by means of an intramuscular injection of pentobarbital. Lizards were fixed in a 10% aqueous formaldehyde solution for 48h, rinsed and transferred to a 70% ethanol solution. Specimens were scanned using an X-Tek HMX 160 µCT system (Nikon, X-Tek Systems Ltd, UK) at a voxel size of 24.90 µm with the following parameters: X-ray voltage, 90 kV; X-ray intensity, 70 µA; exposure time, 2000 ms; number of projections, 2500. Scans were segmented using Avizo 9.0 (Thermo Fischer Scientific) and 3D surfaces of the cranium and mandible were reconstructed and exported separately.

Geometric morphometrics

Anatomical landmarks were placed on the left side of the skull and mandible in Idav Landmark 3.6 (Institute for Data Analysis and Visualization, University of California, Davis). Each hemi-mandible was defined by 33 anatomical landmarks, and each half of the cranium by 47 landmarks (Table 1). In addition, 54 and 49 semi-landmarks on curves were digitized on the cranium and mandible, respectively (Figures 1, 2). The set of points was chosen to describe the whole three-dimensional structure, focusing on areas of muscle insertion (e.g., the quadrate, the lateral side of the mandible) and other areas potentially relevant from a mechanical perspective (e.g., the shape of the snout, the curvature of the mandible). Sliding semi-landmarks were projected onto the surface using a thin-plate spline deformation (Gunz & Mitteroecker, 2013) and slid. Next, three iterations of thin-plate spline relaxation were performed against a Procrustes consensus, using the library "Morpho" (Schlager, 2013). Anatomical landmarks and curves of the skull were mirrored across the sagittal plane ("mirrorfill" function from "paleomorph" package) (Cardini, 2016; 2017).

Musculature

After scanning, cranial muscles were dissected on the left side of the skull of each specimen, blotted dry and weighed using a digital balance (Mettler AE100; ± 0.1 mg). Muscle volume was obtained by dividing muscle mass by density (1.06 $g.cm^{-3}$; Mendez & Keys, 1960). Muscles were immerged in an aqueous solution of nitric acid (30%) for 20 to 24 hours to digest the connective tissues and to separate muscle fibers. Muscles were then transferred into a 50% aqueous glycerol solution to stop the reaction. Approximately 10 muscle fibers per muscle were randomly selected, and drawn using a camera lucida mounted on a Leica binocular scope. Drawings including a scale bar were scanned and muscle fiber lengths were measured using Image J 1.52 (National Institutes of Health, USA). The physiological cross-sectional area (PCSA) of each muscle was calculated by dividing muscle volume by the mean fiber length. We identified 12 jaw muscle bundles representing five functional groups. The

jaw openers included *m. depressor mandibulae* (mDM). The group of the external adductors included the *m. adductor mandibulae externus pars superficialis anterior* (mAMESA) and *posterior* (mAMESP), the *pars medialis* (mAMEM), and the *produndus* (mAMEP). The *M. adductor mandibulae posterior* (mAMP) was considered part of this group although it is not an external adductor *sensu stricto*. The group of the pseudotemporalis muscles was composed of *m. pseudotemporalis superficialis* (mPSTS) and *profundus* (mPSTP). The pterygoids included *m. pterygoideus pars lateralis* (mPTL) and *medialis* (mPTM), while the constrictor dorsalis muscles encompassed the *m. levator pterygoidei* (mLPT) and *m. protractor pterygoidei* (mPPT).

Statistical analyses

All statistical analyses were performed using R (R Core Team, 2020). Bite force and muscle data were $\log_{10}$-transformed, proportions of the type of food consumed (e.g., plants, hard arthropods) were arcsine-transformed, and the homogeneity of variances and normality of the distribution of the residuals were verified using Bartlett and Shapiro tests, respectively. For analyses including phylogeny we used a previously published tree describing the relationships between the populations in this study system (see Taverne et al. 2020). Preliminary genomic analyses (Sabolić et al. in preparation) indicated that there is effectively no gene flow between populations, and thus treating them as independent evolving lineages for phylogenetic comparative analyses is justified. Mentions of residual data in all subsequent analyses refer to the residuals of the variables extracted from simple or multivariate regressions on size (more specifically, the centroid size of the skull) performed on the sub-dataset considered (e.g., all females, or females of a single species).

The effect of sex and species on the muscle architecture variables (including the summed muscle mass, the average fiber length, and the summed PCSA of each muscle group) was investigated by means of a two-way multivariate analysis of covariance (MANCOVA, “mancova” function, “jmv” package) with the centroid size of the skull (Csize) as co-variable. MANCOVAs with Csize as co-variable were subsequently performed to test for differences between sexes and localities within each species. Permutation tests were performed (1000 iterations, with randomization of the residuals) to examine the effect of Csize (of the skull or the mandible, depending on the situation), sex, and species, and the effect of Csize, sex, and locality on the mandible and skull shape, using the function “procD.lm” function (“geomorph” package).

Next, muscle and morphological data were averaged by population and by sex. Relationships between all muscle variables (mass, fiber length, and PCSA), bite force, the proportion of plants consumed, the proportion of hard prey consumed, and sexual dimorphism in head dimensions were investigated in males and females separately given the known sexual dimorphism in these species. To

do so, stepwise regressions were performed either on raw or on residual muscular data (generated by regressing traits against skull Csize) using the function “stepAIC”, or using the function “phylostep” (“phylolm” package) when accounting for phylogeny.

The contribution of allometry to the observed variability in shape was estimated using a Procrustes ANOVA with permutation (“procD.lm” function) which tested the relationship between the Procrustes coordinates and the centroid size of either the skull or the mandible of each specimen (the “procD.pgls” function was used when including phylogeny).

The relationships between mandible or skull shape and muscle variables, muscle residual variables (obtained after multiple regressions on skull Csize or mandible Csize), bite force, residual bite force, and ecological variables were assessed by running two-block partial least-squares (2b-PLS) regressions using the function “two.b.pls” (“geomorph” package), or using the function “phylo.integration” (“geomorph” package) when accounting for phylogeny. The contributions of the variables included in the tested block to the covariation axis were extracted. Then, these interspecific patterns of covariation between morphology, musculature, performance, and ecology were compared with those occurring at the intraspecific level. To do so, additional 2b-PLS regressions were computed for each sex in each species. The coefficient of correlation between scores of projected values on the first singular vectors of the two blocks (rPLS), accounting for the strength of the covariation axis, was extracted for each 2b-PLS regression. The rPLS of 2b-PLS regressions performed at different levels (intra or interspecific) were compared using the function “compare.pls” (“geomorph” package).

Finally, additional two-block partial least-squares regressions were used to investigate the relationships between the residual muscular variables (again, obtained by a regression on mandible or skull Csize), diet variables, and the allometry-free (AF) mandible and skull shape (obtained with the functions “CAC” and “showPC” - “morpho” package). The covariation patterns at the inter and intraspecific levels were compared as detailed previously. All shape changes associated with the covariation patterns were extracted using the function “tps3d” (“morpho” package).

Results

Inter-population variability in muscle architecture and shape

The results of the two-way MANCOVAs carried out on the muscle architecture variables are summarized in Table 2 and show that muscle architecture differs between sexes and species. The effect of Csize was also significant. A significant interaction between sex and species was also detected prompting us to run analyses for each species separately. A subsequent MANCOVA found

219 significant sex, locality, and Csize effects for *P. melisellensis*. No interaction between sex and locality
220 was detected. The same patterns were detected for *P. sicula* (Table 2).

221 The results of the permutation analyses carried out on cranial and mandible shape are summarized in
222 Table 3, and variability in morphology within the dataset is illustrated in Supplementary Information
223 1. The tests performed on the mandible shapes of all specimens revealed significant effects of Csize,
224 sex, species, and the interaction between Csize and species. In *P. melisellensis*, significant effects of
225 Csize, sex, locality, and the interaction between Csize and locality were detected. In *P. sicula,*
226 significant effects of Csize, sex, and locality were detected, as well as interaction effects between
227 Csize and sex, and between sex and locality. The permutation tests, performed on the skull shape of
228 all specimens showed an effect of Csize, sex, species, as well as the interaction between Csize and
229 species, and between sex and species. In *P. melisellensis*, the tests revealed an effect of Csize, sex
230 and locality, and the interaction between sex and locality. In *P. sicula*, the tests revealed an effect of
231 Csize, sex and locality, and the interaction between Csize and sex.

232 *Relationships between muscle architecture, bite force, and ecology*

233 The physiological cross-sectional area (PCSA) of the jaw muscles explained variation in bite force
234 (Table 4). In females, greater absolute (R^2 = 0.85, P < 0.001) and residual (R^2 = 0.71, P = 0.001) bite
235 force was associated with relatively stronger external adductors and weaker pseudotemporalis
236 muscles. In males an increase in absolute bite force (R^2 = 0.30, P = 0.04) was associated with stronger
237 external adductors and weaker pterygoid muscles. These results held when accounting for
238 phylogeny.

239 The proportion of plants consumed was also significantly correlated with the absolute and relative
240 PCSA of jaw adductor muscles in both females and males (absolute data in females: R^2 = 0.54, P =
241 0.012; in males: R^2 = 0.53, P = 0.013; residual data in females: R^2=0.42, P = 0.013; in males R^2=0.42, P
242 = 0.037). In females, a higher proportion of plants in the diet was associated with relatively stronger
243 pseudotemporalis muscles and weaker pterygoids. In males an increase in the amount of plant
244 material in the diet was associated with relatively stronger jaw openers and external adductors, and
245 relatively weaker pterygoids and constrictor dorsalis muscles. These results were largely upheld
246 when accounting for phylogeny (Table 4).

247 The multiple regressions also revealed a significant association between the proportion of hard prey
248 items consumed and the PCSA of the jaw muscles in females (R^2 = 0.43, P = 0.033) and residual PCSA
249 in both females and males (females: R^2 = 0.44, P = 0.030; males: R^2 = 0.57, P = 0.008). In females, a
250 greater proportion of hard prey was associated with stronger pterygoids and relatively weaker

external adductors. In males, the same pattern was observed but the PCSA of the pseudotemporalis muscles was also associated with an increase in hard prey in the diet. Despite some small differences, the results of these regressions remained consistent when accounting for phylogeny (Table 4).

The sexual dimorphism in head dimensions, which was considered here as a proxy for the intensity of sexual competition, correlated with the absolute PCSA of the jaw muscles in both females ($R^2 = 0.54$, $P = 0.004$) and males ($R^2 = 0.29$, $P = 0.040$). In females, a higher dimorphism was associated with weaker pterygoid muscles, whereas it was associated with weaker pseudotemporalis muscles and stronger jaw openers in males. When accounting for phylogeny, a higher dimorphism correlated with relatively stronger pseudotemporalis muscles in both females and males, and with relatively stronger pterygoids in males (Table 4).

Allometry

Allometry explained a significant part of the variability in skull and mandible shape in males and females at the intra and interspecific levels (Table 5). For example, allometry explained 13.4% and 18.0 % of the total variation in mandible and cranium shape, respectively (all $P = 0.001$). In males, allometry explained 9.7% and 7.1 % of the total variation in mandible and cranial shape (all $P = 0.001$). When accounting for phylogeny, allometries were no longer significant ($P > 0.05$). Although they were significant, allometry trajectories did not differ much between species (Supplementary Information 2).

Co-variation between head shape, performance, muscle architecture, and ecology

For both sexes of each species, the 2b-PLS analyses at the interspecific level revealed that mandible and cranial shapes significantly covaried with bite force (except in males), muscular, and ecological variables (Table 6). Most patterns of covariation still held when accounting for the phylogeny. Residual musculature variables and ecology also strongly covaried with cranial and mandible shape corrected for allometry, in both females and males, even when correcting for phylogeny (except in a few cases, see Table 6). The PCSA and the volume of three muscle groups, the external adductors, the pseudotemporalis muscles and the pterygoids were the muscular variables that drove this covariation (Supplementary Information 3). On the other hand, the proportion of plants consumed was the ecological variable that best explained the covariation between ecology and cranial shape. In all cases, the shapes associated with bigger and stronger muscles were similar to those associated with a higher proportion of plants consumed. Specifically, an increase in muscle PCSA as well as an increased consumption of plants were both associated with an increased overall robustness of the mandible, with larger areas for muscle insertions (e.g., the coronoid process as the insertion site for

pseudotemporalis muscles, or the lateral side of the mandible serving as an attachment site for external adductors). Additionally, the snout was pointier, the skull was taller (mostly due to a more pronounced ventral curvature of the pterygoid bone), and presented a wider temporal window and a more curved quadrate (Figure 3).

No pattern of covariation was detected between residual bite force and shape or residual bite force and allometry-free shape, whereas a few significant patterns were detected between residual musculature and cranial or mandible shape (Table 6). For instance, the skull shape of males covaried with residual jaw musculature (especially the PCSA and the volume of the external adductors, the pseudotemporalis muscles and the pterygoids, see Supplementary Information 3). The skull shape variation was somewhat similar to that described above, except that the increase in skull height was enabled by a rounder skull roof instead of having a more ventrally curved pterygoid bone. Residual musculature variables and ecological variables also covaried with allometry-free skull and mandible shape (Table 6), yet covariation patterns differed by sex. In females, stronger and larger constrictor dorsalis muscles were associated with a narrower posterior section of the skull, characterized by quadrates and posterior processes of the parietals pushed towards the midsagittal plane. In males, relatively stronger and bigger external adductors, pseudotemporalis muscles, and pterygoids were associated with a more robust mandible, a bigger coronoid process, and taller skull roof, a more ventrally curved pterygoid bone, and a shorter snout. In males, similar deformations were observed associated with an increase in the proportion of hard items in the diet (Figure 4). Similar patterns were generally detected when accounting for the phylogeny (Table 6).

Comparison of the evolutionary trajectories

The rPLS of each 2b-PLS were compared to explore whether the strength of the patterns of covariation was similar between sexes, species, and at the intra- (Supplementary Information 4) and interspecific levels (Table 6, 7). Overall, we found no or little statistical difference in the strength of the covariation. The nature of the covariations between ecology, muscles architecture and morphology also appeared qualitatively similar, as illustrated by the comparison in covariation pattern between muscle architecture and skull shape in males of *P. melisellensis* and in all males, for example (Figure 5). Indeed, the increase in the same set of muscle architecture variables (the mass and PCSA of the adductor muscle groups) contributes to similar morphological variation (a wider temporal window, enabled by a higher skull roof, a pterygoid bone that is more ventrally and medially curved, a more curved quadrate, a more vertical jugal).

Discussion

Differences in selective regimes across independent insular populations

The populations included in the present study vary greatly in their ecology as they inhabit islands that differ in their size and habitat structure (Taverne et al. 2019). Island area and island isolation further influence the diversity and the abundance of resources available, predation pressure, and population densities which together drive ecological dynamics (Novosolov & Meiri, 2013; Novosolov et al. 2016, Whittaker et al. 2017; Itescu et al. 2019). In the Adriatic archipelago, the lizard populations present dietary specializations, ranging from a strictly insectivorous diet to an omnivorous diet including a majority of plant items (Taverne et al. 2019). The consumption of mechanically resistant items (e.g., hard arthropods, plant material) was observed on the smallest and the most depauperate islands. These populations also vary in the intensity of sexual competition, as expressed by the level of sexual dimorphism in head dimensions. Ecological pressures such as sexual competition and the consumption of difficult-to-reduce items are reflected in variation in bite force (Taverne et al. 2020). Additionally, these factors impact muscular anatomy and cranial shape. These patterns differed depending on the trait considered (Tables 4 and 6, Figures 3 and 4), suggesting that different selective regimes operate on these islands. Because different associations between form and function were detected in males and females, sexes appear to be confronted with different selective pressures. Interestingly sex-related specificities were replicated among populations within a species, but were species-specific.

Evolution of phenotypes

The present study allowed us to partly tease apart the drivers of phenotypic variation. Lizards grow continuously during their life (Haines, 1969). For this reason, size is often a central life-history trait enabling rapid responses to environmental fluctuations (Meiri, 2007; Hall & Warner, 2017), especially in insular habitats (Lomolino, 2005; Losos & Ricklefs, 2009; Sagonas et al. 2014). A significant part of phenotypic variation often originates from allometric growth in ectotherms like lizards (Urošević et al. 2012a,b). As expected, our results showed that phenotypic variation across populations and sexes was partly explained by allometry (Table 5). Interspecific differences observed here are congruent with diversification along the allometric trajectory (Felsenstein, 1985). Besides allometry, dietary specialization, the intensity of sexual competition, and bite force were important drivers of phenotypic variation.

We found that musculature strongly drives variation in bite force in the two species studied. Moreover, our analyses suggest that this relationship is not purely allometric. An increase in bite force was associated with an increase in the absolute and the relative PCSA of the external jaw adductors in both males and females (Table 4) suggesting that increasing the force of this muscle

group is the most effective way to induce variation in bite force. This is corroborated by previous studies that showed that the external adductor muscles of lizards are the primary drivers of variation in bite force at the interspecific level (Wittorski et al. 2016). In males, the variation in the contribution of the external adductors is largely the result of the variation in muscle volume (Supplementary Information 5). As these muscles are positioned laterally in the head, their volume might be less constrained by other cranial structures than deeper muscle bundles (Rieppel & Gronowski, 1981; Herrel et al. 1998; Herrel et al. 2007). Functionally relevant associations between musculature and ecology were also detected. The inclusion of greater amounts of plant items in the diet was associated either with stronger pseudotemporalis muscles in females, or with stronger external adductors in males, whereas greater amounts of hard prey in the diet were associated with stronger pterygoids in both sexes. The pterygoids are more efficient at generating bite force at large gape as their moment arm increases significantly with gape (Herrel et al. 1999 a,b). Hence, dietary specialization seems to be allowed by a preferential investment in muscle groups that optimize force generation in a context of biting at low or wide gapes (when eating plant items or hard prey, respectively). The same logic seems to operate in males, with more intense sexual competition, such as male-male combat, going along with more strongly developed pterygoid muscles.

Our analyses of covariation revealed strong associations between ecology, bite force, and muscle architecture on the one hand, and mandible and cranial shape on the other hand. However, the fact that residual bite force and muscle variables only rarely showed significant covariation with shape highlights the influence of size, as corroborated by the significant allometry in the shape of the mandible and cranium in both males and females. The importance of allometric effects in allowing skull shape changes in relation to habitat use is common in lizards (at the intraspecific level: Kaliontzopoulou, Carretero & Llorente, 2010; at the interspecific level: Urošević et al. 2012a). Yet, residual data showed covariations with allometry-free mandible and cranial shapes, indicating that variation in shape is not explained by allometry alone. Instead, it appears that the covariation between bite force and morphology is explained primarily by size effects and allometry, whereas muscle forces appear to covary with shape corrected for allometry. Thus, shape variation beyond that imposed by overall size variation seems to reflect local constraints imposed by the development of more forceful jaw muscles in these lizards. We identified two types of shape variation patterns associated with variation in other traits. The first type includes covariation patterns that are functionally related to muscle packing constraints (e.g., the height of skull roof, the robustness of the coronoid process), while the second includes patterns (e.g., the height of the snout, the ventral curvature of the mandible) likely reflecting the mechanical constraints associated with the distribution of strains throughout the masticatory system. Biomechanical models aiming at

understanding the functional and mechanical consequences of the observed morphological variation are needed to fully understand the observed patterns, however.

At present we cannot demonstrate that the observed patterns are convergent at the intra and interspecific level in this island system. This is because, to our knowledge, no reliable statistical tool exists to directly test for convergence in the association between groups of continuous multivariate traits (such as shape and the ecological variables used in the present study; but see Bergmann & McElroy, 2014 for a possible approach).

From micro to macroevolution in an island radiation

The comparison of the rPLS (Table 7) and the qualitative description of the evolutionary trajectories suggest that patterns of intraspecific variation are replicated at the interspecific level. In other words, we showed that under similar ecological circumstances, predictable response in musculature occurs, and that in turn, variation in muscle architecture is associated with similar patterns of morphological variation among populations and among species. Such consistency between hierarchical levels of biological integration was proposed to be the result of selection (Calsbeek, Knouft & Smith, 2006), and likely to underlie the genesis of phenotypic diversity (Kaliontzopoulou, Pinho & Martinez-Freiria, 2018). Gould (1989) proposed that evolution is the result of selection plus contingency rendering convergence less likely in more distantly related organisms. Additionally, Blount and co-authors (2018) showed that repeatable evolution of traits is more likely to occur in closely related lineages as is observed in our study comparing two species of the same genus. Put another way, the power of selection to produce convergent phenotypes in similar ecological contexts decreases in distant taxa because of the genetic differences that accumulate over time, while the power of contingency increases**.** The patterns of covariation described here suggest that at least part of the hypothesis is true. Whether this can be extrapolated to the genus or even family level remains to be tested, however.

Main conclusions

The relationships between head dimensions, bite force, and ecology at the interspecific level have received great attention over the past decades. The weak link between morphology and diet at the intraspecific level has been proposed to be caused by the prevalence of other agents of selection such as intraspecific competition and the need for food partitioning (Schoener, 1967; Herrel et al. 1999, Vanhooydonck et al. 2010), or sexual selection through male-male combat (Sagonas et al. 2014; Lopez-Darias et al. 2015; Donihue et al. 2016). Using insular *Podarcis* lizards as a model system, we demonstrated that diet and sexual competition are both important drivers of phenotypic diversity

414 at the intra- and interspecific level. However, phenotypic evolution is sometimes fluctuating and may
415 only rarely be translated into long-term directional change (Gibbs & Grant, 1987; Hairston & Dillon,
416 1990; Ellner et al. 1999; Grant & Grant, 2006). The present study shows that ecological pressures at
417 the population level are strong enough to allow the emergence of macroevolutionary patterns of
418 variation across the Adriatic thus linking population-level processes to interspecific patterns of
419 variation.

420 **References**

421 Adams DC, Otárola-Castillo E. **2013**. geomorph: an R package for the collection and analysis of
422 geometric morphometric shape data. *Methods in Ecology and Evolution* **4**: 393-399.

423 Altshuler DL, Bahlman JW, Dakin R, Gaede AH, Goller B, Lentink D, Segre PS, Skandalis DA. **2015**. The
424 biophysics of bird flight: functional relationships integrate aerodynamics, morphology, kinematics,
425 muscles, and sensors. *Canadian Journal of Zoology* **93**: 961-975.

426 Baeckens S, Van Damme R. **2020**. The island syndrome. *Current biology* **30**: 338-339.

427 Barel CD, Anker GC, Witte F, Hoogerhoud RJ, Goldschmidt T. **1989**. Constructional constraint and its
428 ecomorphological implications. *Acta morphologica neerlando-scandinavica* **27**: 83-109.

429 Bergmann PJ, McElroy EJ. **2014**. Many-to-many mapping of phenotype to performance: an extension
430 of the F-matrix for studying functional complexity. *Evolutionary Biology* **41**: 546-560.

431 Boag PT, Grant PR. **1981**. Intense natural selection in a population of Darwin's finches (Geospizinae)
432 in the Galapagos. *Science* **214**: 82-85.

433 Bookstein FL. **1977**. Introductory review: The study of shape transformation after D'Arcy Thompson.
434 *Mathematical Biosciences* **34**: 177-219.

435 Brecko J, Huyghe K, Vanhooydonck B, Herrel A, Grbac I, Van Damme R. **2008**. Functional and
436 ecological relevance of intraspecific variation in body size and shape in the lizard *Podarcis*
437 *melisellensis* (Lacertidae). *Biological Journal of the Linnean Society* **94**: 251-264.

438 Calsbeek R, Knouft JH, Smith TB. **2006**. Variation in scale numbers is consistent with ecologically
439 based natural selection acting within and between lizard species. *Evolutionary Ecology* **20**: 377-394.

Campbell-Staton SC**,** Cheviron ZA, Rochette N, Catchen J, Losos JB, Edwards SV. **2017**. Winter storms drive rapid phenotypic, regulatory, and genomic shifts in the green anole lizard. Science **357**: 495-498.

Cardini A. **2016**. Lost in the other half: improving accuracy in geometric morphometric analyses of one side of bilaterally symmetric structures. *Systematic Biology* **65**: 1096-1106.

Cardini A. **2017**. Left, right or both? Estimating and improving accuracy of one-side-only geometric morphometric analyses of cranial variation. *Journal of Zoological Systematics and Evolutionary Research* **55**: 1-10.

Cornette R, Tresset A, Herrel A. **2015**. The shrew tamed by Wolff's law: Do functional constraints shape the skull through muscle and bone covariation? *Journal of morphology* **276**: 301-309.

Cooper WE Jr, Vitt LJ. **2002**. Distribution, extent, and evolution of plant consumption by lizards. *Journal of Zoology, London* **257**: 487-517.

Currey JD. **2002**. The structure of bone tissue. In: Currey JD, ed. *Bones: Structure and mechanics*. Princeton University Press, New Jersey, USA, 3-26.

Cheverud JM. **1982**. Phenotypic, genetic, and environmental morphological integration in the cranium. *Evolution* **36**: 499-516.

Da Silva FO, Fabre AC, Savriama Y, Ollonen J, Mahlow K, Herrel A, Müller J, Di-Poï N. **2018**. The ecological origins of snakes as revealed by skull evolution. *Nature communications* **9**: 1-11.

D'Arcy Thompson. **1942**. *On growth and form.* Cambridge University Press.

Donihue CM, Brock KM, Foufopoulos J, Herrel A. **2016**. Feed or fight: testing the impact of food availability and intraspecific aggression on the functional ecology of an island lizard. *Functional Ecology* **30**: 566-575. doi: 10.1111/1365-2435.12550

Donihue CM, Herrel A, Fabre AC, Kmath A, Geneva AJ, Schoener TW, Kolbe JJ, Losos JB. **2018**. Hurricane-induced selection on the morphology of an island lizard. *Nature* **560**: 88-92.

Downes S, Bauwens D. **2002**. An experimental demonstration of direct behavioural interference in two Mediterranean lacertid lizard species. *Animal Behaviour* **63**: 1037-1046.

Ellner S, Hairstone NG, Kearns CM, Babaï D. **1999**. The roles of fluctuating selection and long-term diapause in microevolution of diapause timing in a fresh-water copepod. *Evolution* **53**: 111-122.

Fabre AC, Andrade DV, Huyghe K, Cornette R, Herrel A. **2014a**. Interrelationships between bones, muscles, and performance: biting in the lizard *Tupinambis merianae*. *Evolutionary Biology* **41**: 518-527.

Fabre AC, Bardua C, Bon M, Clavel J, Felice RN, Streicher JW, Bonnel J, Stanley EL, Blackburn DC, Goswami A. **2020**. Metamorphosis shapes cranial diversity and rate of evolution in salamanders. *Nature Ecology and Evolution* **4**:1129-1140.

Fabre AC, Cornette R, Huyghe K, Andrade DV, Herrel A. **2014b**. Linear versus geometric morphometric approaches for the analysis of head shape dimorphism in lizards. *Journal of Morphology* **275**: 1016-1026.

Fabre AC, Dowling C, Portela Miguez R, Fernandez V, Noirault E, A Goswami. **2021**. Functional constraints during development limit jaw shape evolution in marsupials. *Proceedings of the Royal Society B* **288**: 20210319.

Fabre AC, Perry JM, Hartstone-Rose A, Lowie A, Boens A, Dumont M. **2018**. Do muscles constrain skull shape evolution in Strepsirrhines? *The Anatomical Record* **301**: 291-310.

Fish FE. **1998**. Comparative kinematics and hydrodynamics of odontocete cetaceans: morphological and ecological correlates with swimming performance. *Journal of Experimental Biology* **201**: 2867-2877.

Fish FE, Howle LE, Murray MM. **2008**. Hydrodynamic flow control in marine mammals. *Integrative and Comparative Biology* **48**: 788-800.

Gibbs HL, Grant PR. **1987**. Oscillating selection on Darwin's finches. *Nature* **327**: 511-513.

Goodwin BC, Trainor LEH. **1980**. A field description of the cleavage process in embryogenesis. *Journal of Theoretical Biology* **85**: 757-770.

Gould SJ. **1989**. In: "A wonderful life: The Burgess Shale and the Nature of History". WW Norton and Company, USA.

492 Gould SJ, Lewontin RC. **1979**. The spandrels of San Marco and the Panglossian paradigm: a critique of
493 the adaptationist programme. *Proceedings of the royal society of London Series B Biological Sciences*
494 **205**: 581-598.

495 Grant PR, Grant BR. **2006**. Evolution of character displacement in Darwin's finches. *Science* **313**: 224-
496 226.

497 Gunz P, Mitteroecker P. **2013**. Semilandmarks: a method for quantifying curves and surfaces. *Hystrix,*
498 *the Italian journal of mammalogy* **24**: 103-109.

499 Gunz P, Mitteroecker P, Bookstein FL. **2005**. Semilandmarks in three dimensions. In Slice DE, ed.
500 *Modern morphometrics in physical anthropology,* Springer, Boston, MA, 73-98.

501 Hairstone NG, Dillon TA. **1990**. Fluctuating selection and response in a population of freshwater
502 copepods. *Evolution* **44**: 1796-1805.

503 Hedenström A. **2002**. Aerodynamics, evolution and ecology of avian flight. *Trends in Ecology &*
504 *Evolution* **17**: 415-422.

505 Hedenström A, Johansson LC. **2015**. Bat flight: aerodynamics, kinematics and flight
506 morphology. *Journal of Experimental Biology* **218**: 653-663.

507 Herrel A, Aerts P, De Vree F. **1998**. Static biting in lizards: functional morphology of the temporal
508 ligaments. *Journal of Zoology* **244**: 135-143.

509 Herrel A, Spithoven L, Van Damme R, De Vree F. **1999a**. Sexual dimorphism of head size in *Gallotia*
510 *galloti*: testing the niche divergence hypothesis by functional analyses. *Functional Ecology* **13**: 289-
511 297.

512 Herrel A, De Grauw ED, Lemos-Espinal JA. **2001**. Head shape and bite performance in Xenosaurid
513 lizards. *Journal of Experimental Zoology* **290**: 101-107.

514 Herrel A, Joachim R, Vanhooydonck B, Irschick DJ. **2006**. Ecological consequences of ontogenetic
515 changes in head shape and bite performance in the Jamaican lizard *Anolis lineatopus*. *Biological*
516 *Journal of the Linnean Society* **89**: 443-454.

Herrel A, Schaerlaeken V, Meyers JJ, Metzger KA, Ross CF. **2007**. The evolution of cranial design and performance in squamates: consequences of skull-bone reduction on feeding behavior. *Integrative and Comparative Biology* **47**: 107-117.

Herrel A, McBrayer LD, Larson PM. **2007**. Functional basis for sexual differences in bite force in the lizard *Anolis carolinensis*. *Biological Journal of the Linnean Society* **91**: 111-119.

Herrel A, Podos J, Vanhooydonck B, Hendry AP. **2009**. Force–velocity trade-off in Darwin's finch jaw function: a biomechanical basis for ecological speciation? *Functional Ecology* **23**: 119-125.

Herrel A, Moore JA, Bredeweg EM, Nelson NJ. **2010**. Sexual dimorphism, body size, bite force and male mating success in Tuatara. *Biological Journal of the Linnean Society* **100**: 287-292.

Herrel A, Verstappen M, De Vree F. **1999b**. Modulatory complexity of the feeding repertoire in scincid lizards. *Journal of Comparative Physiology A* **184**: 501-518.

Huyghe K, Herrel A, Adriaens D, Tadić Z, Van Damme R. **2009**. It is all in the head: morphological basis for differences in bite force among colour morphs of the Dalmatian wall lizard. *Biological Journal of the Linnean Society* **96**: 13-22.

Kaliontzopoulou A. **2011**. Geometric morphometrics in herpetology: modern tools for enhancing the study of morphological variation in amphibians and reptiles. *Basic and Applied Herpetology* **25**: 5-32.

Kaliontzopoulou A, Carretero MA, Llorente GA. **2010**. Intraspecific ecomorphological variation: linear and geometric morphometrics reveal habitat-related patterns within *Podarcis bocagei* wall lizards. *Journal Evolutionary Biology* **23**: 1234-1244.

Kaliontzopoulou A, Pinho C, Martinez-Freiria F. **2018**. Where does diversity come from? Linking geographical patterns of morphological, genetic, and environmental variation in wall lizards. *BMC Evolutionary Biology* **18**: 124-136.

Klingenberg CP. **2002**. Morphometrics and the role of the phenotype in studies of the evolution of developmental mechanisms. *Gene* **287**: 3-10.

Klingenberg CP. **2011**. MorphoJ: an integrated software package for geometric morphometrics. *Molecular Ecology Resources* **11**: 353-357.

543 Kueffer C, Drake DR, Fernández-Palacios JM. **2014**. Island biology: looking towards the future. *Biology*
544 *Letters* **10**: 20140719.

545 Lande R. **1976**. Natural selection and random genetic drift in phenotypic evolution. *Evolution* **30**: 314-
546 334.

547 Lappin AK, Hamilton PS, Sullivan BK. **2006**. Bite-force performance and head shape in a sexually
548 dimorphic crevice-dwelling lizard, the common chuckwalla [*Sauromalus ater* (= *obesus*)]. *Biological*
549 *Journal of the Linnean Society* **88**: 215-222.

550 Lappin AK, Husak JF. **2005**. Weapon performance, not size, determines mating success and potential
551 reproductive output in the collared lizard (*Crotaphytus collaris*). *The American Naturalist* **166**: 426-
552 436.

553 Lopez-Darias M, Vanhooydonck B, Cornette R, Herrel A. **2015**. Sex-specific differences in
554 ecomorphological relationships in lizards of the genus *Gallotia*. *Functional Ecology* **29**: 506-514.

555 Losos JB. **1990**. Ecomorphology, performance capability, and scaling of West Indian *Anolis* lizards: an
556 evolutionary analysis. *Ecological Monographs* **60**: 369-388.

557 Losos JB. **2009**. *Lizards in an evolutionary tree. Ecology and Adaptive radiation of Anoles*. University
558 of California Press, CA.

559 Losos JB, Ricklefs RE. **2009**. Adaptation and diversification on islands. *Nature* **457**: 830-836.

560 Marroig G, Cheverud JM. **2005**. Size as a line of least evolutionary resistance: diet and adapative
561 morphological radiation in New World Monkeys. *Evolution* **59**: 1128-1142

562 Martin RD, Ross CF. **2005**. The evolutionary and ecological context of primate vision. In Kremers J,
563 ed. *The primate visual system: A comparative approach*, John Wiley & Sons, Ltd 1-36.

564 Massetti F, Kaliontzopoulou A, Gomes V, Rato C. **2018**. Variation in morphology and functional
565 performance across distinct evolutionary lineages of the Moorish gecko (*Tarentola mauritanica*) from
566 the Iberian Peninsula. *Journal of Zoological Systematics and Evolutionary Research* **57**: 431-444.

567 McGlothlin JW, Kobiela ME, Wright HV, Mahler DL, Kolbe JJ, Losos JB, Brodie III ED. **2018**. Adaptive
568 radiation along a deeply conserved genetic line of least resistance in Anolis lizards. *Evolution Letters*
569 **4**: 310-322.

570 Meiri S. **2008**. Evolution and ecology of lizard body sizes. *Global Ecology and Biogeography* **17**: 724-
571 734.

572 Mendez J, Keys A, Anderson JT, Grande F. **1960**. Density of fat and bone mineral of the mammalian
573 body. *Metabolism* **9**: 472-477.

574 Nevo E. **1972**. Competitive exclusion between insular *Lacerta* species (Sauria, Lacertidae). Notes on
575 experimental introductions. *Oecologia* **10**: 183-190.

576 Nikolic B, Josic P, Buric D, Tkalec M, Lisicic D, Blazevic SA, Hranilovic D. **2019**. Coexisting lacertid lizard
577 species *Podarcis siculus* and *Podarcis melisellensis* differ in dopamine brain concentrations. *Journal of*
578 *Comparative Physiology A* **205**: 451-456.

579 Pigliucci M, Kaplan J. **2000**. The fall and rise of Dr Pangloss: adaptationism and the Spandrels paper
580 20 years later. *Trends in ecology & evolution* **15**: 66-70.

581 R Core Team. **2020**. R: A language and environment for statistical computing. R Foundation for
582 Statistical Computing, Vienna, Austria. URL: https://www.R-project.org/.

583 Rieppel O, Gronowski RW. **1981**. The loss of the lower temporal arcade in diapsid reptiles. *Zoological*
584 *Journal of the Linnean Society* **72**: 203-217.

585 Reilly SM, Miles DB, McBrayer LD. **2007**. The evolution of foraging mode paradigm in lizard ecology.
586 In Reilly SM, McBrayer LD, Miles DB, eds. In *Lizard Ecology*, *The evolutionary consequences of*
587 *foraging mode*, **17**, Cambridge University Press.

588 Renaud S, Auffray JC, De la Porte S. **2010**. Epigenetic effects on the mouse mandible: common
589 features and discrepancies in remodelling due to muscular dystrophy and response to food
590 consistency. *BMC evolutionary biology* **10**: 28.

591 Renaud S, Pantalacci S, Auffray JC. **2011**. Differential evolvability along lines of least resistance of
592 upper and lower molars in island house mice. *PlosOne* **6**: e18951

593 Rodrigues HG, Šumbera R, Hautier L. **2015**. Life in burrows channeled the morphological evolution of
594 the skull in rodents: the case of African Mole-Rats (Bathyergidae, Rodentia). *Journal of Mammalian*
595 *Evolution **23***: 175-189.

596 Roscito JG, Rodrigues MT. **2010**. Comparative cranial osteology of fossorial lizards from the tribe
597 Gymnophthalmini (Squamata, Gymnophthalmidae). *Journal of morphology* **271**: 1352-1365.

598 Sagnes P, Gaudin P, Statzner B. **1997**. Shifts in morphometrics and their relation to hydrodynamic
599 potential and habitat use during grayling ontogenesis. *Journal of fish biology* **50**: 846-858.

600 Sagonas K, Pafilis P, Lymberakis P, Donihue CM, Herrel A, Valakos ED. **2014**. Insularity affects head
601 morphology, bite force and diet in a Mediterranean lizard. *Biological Journal of the Linnean Society*
602 **112**: 469-484. doi: 10.1111/bij.12290

603 Schoener TW. **1967**. The ecological significance of sexual dimorphism in size in the lizard *Anolis*
604 *conspersus*. *Science* **155**: 474-477.

605 Schoener TW, Slade JB, Stinson CH. **1982**. Diet and sexual dimorphism in the very catholic lizard
606 genus, *Leiocephalus* of the Bahamas. *Oecologia* **53**: 160-169.

607 Schlager S. **2013**. Morpho: Calculations and visualisations related to Geometric Morphometrics. *R*
608 *package version 0.23* **3**: 195-220.

609 Schluter D. **1996**. Adaptive radiation along genetic lines of least resistance. *Evolution* **50**: 1766–1774.

610 Schluter D. **2002**. The ecology of adaptive radiation. Oxford Univ. Press, Oxford, U.K.

611 Segall M, Herrel A, & Godoy-Diana R. **2019**. Hydrodynamics of frontal striking in aquatic snakes: drag,
612 added mass, and the possible consequences for prey capture success. *Bioinspiration & biomimetics*
613 ***14***: 036005.

614 Segall M, Cornette R, Godoy-Diana R, Herrel A. **2020**. Exploring the functional meaning of head shape
615 disparity in aquatic snakes. *BioRxiv* (preprint).

616 Stuart YE, Campbell TS, Hohenlohe PA, Reynolds RG, Revell LJ, Losos, JB. **2014**. Rapid evolution of a
617 native species following invasion by a congener. *Science **346**:* 463-466.

618 Taverne M, Fabre AC, King-Gillies N, Krajnović, Lisičić D, Martin L, Michal L, Petricioli D, Štambuk A,
619 Tadić Z, Vigliotti C, Wehrle BA, Herrel A. **2019**. Diet variability among insular populations of *Podarcis*
620 lizards reveals diverse strategies to face resource-limited environments. *Ecology and Evolution* **9**:
621 12408-12420.

Taverne M, King-Gillies N, Krajnović, Lisičić D, Mira O, Petricioli D, Sabolić I, Štambuk A, Tadić Z, Vigliotti C, Wehrle BA, Herrel A. **2020**. Proximate and ultimate drivers of variation in bite force in the insular lizards *Podarcis melisellensis* and *Podarcis sicula*. *Biological Journal of the Linnean Society* **131**: 88-108.

Urošević A, Ljubisavljević K, Dušan Jelić, Ivanović A. **2012**. Variation in the cranium shape of wall lizards (*Podarcis spp.*): effects of phylogenetic constraints, allometric constraints and ecology. *Zoology* **115**: 207-216.

Van Damme, R. **1999**. Evolution of herbivory in lacertid lizards: effects of insularity and body size. *Journal of Herpetology* **33**: 663-674.

Vanhooydonck B, Cruz FB, Abdala CS, Moreno Azocar DB, Bonino MF, Herrel A. **2010**. Sex-specific evolution of bite performance in *Liolaemus* lizards (Iguania: Liolaemidae): the battle of the sexes. *Biological Journal of the Linnean Society* **101**: 461-475.

Vanhooydonck B, Herrel A, Van Damme R. **2007**. Interactions between habitat use, behavior, and the trophic niche of lacertid lizards. In: Reilly SM, McBrayer LB, Miles DB, eds. *Lizard Ecology*, **14**, Cambridge University Press, UK.

Verwaijen D, Van Damme R, Herrel A. **2002**. Relationships between head size, bite force, prey handling efficiency and diet in two sympatric lacertid lizards. *Functional Ecology* **16**: 842-850.

Wake MH. **2003**. The skull as a locomotor organ. In Hanken J & Hall BK, eds. *The skull*. University of Chicago Press.

Wake DB, Roth G. **1989**. In Wake DB, Roth G, eds. *Complex organismal functions: integration and evolution in vertebrates*. John Wiley & Sons, Chichester, UK.

Wittorski A, Losos JB, Herrel A. **2016**. Proximate determinants of bite force in *Anolis* lizards. *Journal of anatomy* **228**: 85-95.

Zweers GA. 1979. Explanation of structure by optimization and systematization, *Netherlands Journal of Zoology* **29**: 418-440.

647 **Tables:**

648 **Table 1**: Definitions of the anatomical landmarks (LM)

Skull	LM n°	Mandible
Anterior tip of the premaxillar	1	Anterior tip of the dentary
Most medial anterior part of nasal opening	2	Antero-lateral tip of the coronoid
Dorsal point of nasal at the midline	3	Antero-lateral junction between the angular and the surangular
Lateral dorsal protuberance of nasal	4	Antero-lateral tip of the surangular
Anterior end of the joint between the internasal scales	5	Junction between the dentary, the coronoid and the surangular
Anterior corner of the frontal scale	6	Posterior border of the angular foramen below the coronoid
Antero-lateral corner of the frontal scale	7	Dorso-lateral edge of the coronoid
Postero-lateral corner of the frontal scale	8	Dorsal tip of the coronoid
Posterior corner of the frontal scale	9	Dorsal posterior most constriction of the coronoid
Lateral corner of the fronto-parietal scale	10	Mid distance between landmarks 9 and 11
Anterior corner of the interparietal scale	11	Posterior junction between the coronoid and the surangular
Antero-lateral corner of the interparietal scale	12	Junction between the surangular, the angular and the articular
Postero-lateral corner of the interparietal scale	13	Posterior tip of the retroarticular process
Most posterior part of the junction between parietal and occipital scales	14	Antero-ventral junction between the angular and the articular
Junction between the lacrymal, the maxillar and the prefrontal bones	15	Antero-lateral corner of the articular surface
Ventro-medial tip of the frontal bone	16	Postero-lateral corner of the articular surface
Anterior tip of jugal	17	Medial edge of the retroarticular process
Posterior tip of the maxillar, at the junction with the jugal	18	Maximum of curvature between the points 17 and 19
Antero-lateral tip of the pterygoid, at the junction with the ectopterygoid	19	Postero-medial corner of the articular surface
Posterior tip of the jugal	20	Antero-medial corner of the articular surface
Dorsal tip of the jugal	21	Posterior edge of the adductor fossa
Anterior tip of the squamosal	22	Anterior edge of the adductor fossa
Anterior part of the junction between the epipterygoid and the pterygoid	23	Hollow between the posterior and the medial ridges of the coronoid
Dorsal tip of the epipterygoid	24	Postero-ventral tip of the medial ridge of the coronoid
Maximum of curvature of the alar process of prootic	25	Dorsal tip of the medial ridge of the coronoid
Maximum of curvature of the anterior semi-circular canal	26	Dorso-medial tip of the coronoid
Anterior tip of the alar process of sphenoid	27	Antero-ventral tip of the medial ridge of the coronoid
Dorsal tip of the alar process of sphenoid	28	Maximum of curvature of the ventro-medial hollow of the coronoid
Lateral maximum of curvature of the crista prootica	29	Junction between the prearticular, the angular and the splenial
Medial tip of the jugal, at the junction with the ectopterygoid	30	Antero-medial tip of the coronoid
Ventral tip of the postorbital	31	Posterior edge of the Meckelian foramen
Posterior tip of the pterygoid	32	Anterior edge of the Meckelian foramen
Posterior tip of the squamosal	33	Dorso-anterior tip of the dentary
Posterior tip of the paroccipital process of the parietal	34	
Posterior most point of the parietal at the midline	35	
Maximum of curvature of the posterior ridge of the occipital	36	
Ventral bead surrounding the fenestra ovalis	37	
Junction between the vomer and the premaxillar	38	
Anterior junction between the palatin and the maxillar	39	
Posterior junction between the palatin and the maxillar	40	
Anterior tip of the ectopterygoid, at the junction with the maxillar	41	
Posterior tip of the palatin, at the junction with the pterygoid	42	
Postero-medial tip of the ectopterygoid, at the junction with the pterygoid	43	
Anterior tip of the basipterygoid process	44	
Posterior tip of the basipterygoid process	45	
Lateral process of the basioccipital	46	
Lateral process of the basioccipital	47	
Top of the medial parasagittal bead of the quadrate	48	
Antero-ventro-medial tip of the quadrate	49	
Antero-ventro-medial tip of the quadrate	50	
Maximum of curvature of the anterior face of the quadrate	51	
Postero-ventro-lateral tip of the quadrate	52	
Postero-ventro-medial tip of the quadrate	53	
Postero-dorsal tip of the quadrate, at the junction with the supratemporal	54	

649

650 **Table 2**: Results of the analyses of covariance carried out on muscle architecture data at the
651 individual level, either on the whole dataset or for each species separately (df: degrees of freedom,
652 P: P-value). Bold values are statistically significant.

653

		Wilk's λ	F	df	*P*
Entire data set	Species	0.490	8.77	1	**0.001**
	Sex	0.280	21.85	1	**0.001**
	Csize	0.340	16.50	138	**0.001**
	Species x Sex	0.780	2.38	1	**0.006**

		Wilk's λ	F	df1	*P*
P. melisellensis	Locality	0.005	3.17	9	**0.001**
	Sex	0.110	29.10	1	**0.001**
	Csize	0.640	2.01	79	**0.036**
	Locality x Sex	0.220	1.30	5	0.080

		Wilk's λ	F	df1	*P*
P. sicula	Locality	0.013	2.76	5	**0.001**
	Sex	0.240	7.33	1	**0.001**
	Csize	0.350	4.24	58	**0.001**
	Locality x Sex	0.190	0.96	5	0.610

654

Table 3: Results of the permutation tests carried out on shape data at the individual level, either on the whole dataset or for each species separately (df: degrees of freedom, R^2: coefficient of determination, F: F statistic, Z: effect sizes based on F distribution, *P*: P-value). Bold values are statistically significant (< 0.05).

		Skull					Mandible				
		df	R^2	F	Z	*P*	df	R^2	F	Z	*P*
Whole dataset	Csize	1	0.213	41.78	7.66	**0.001**	1	0.265	56.92	8.11	**0.001**
	species	1	0.059	11.73	5.55	**0.001**	1	0.067	14.47	6.85	**0.001**
	sex	1	0.016	3.06	2.60	**0.010**	1	0.027	5.79	4.84	**0.001**
	Csize:species	1	0.012	2.36	2.09	**0.031**	1	0.013	2.74	2.89	**0.004**
	Csize:sex	1	0.007	1.42	0.97	0.177	1	0.006	1.21	0.71	0.232
	species:sex	1	0.012	2.44	2.27	**0.019**	1	0.007	1.56	1.36	0.088
	Csize:species:sex	1	0.011	2.08	1.75	0.058	1	0.005	0.98	0.10	0.454
P. melisellensis	Csize	1	0.272	40.79	6.78	**0.001**	1	0.347	62.47	7.37	**0.001**
	sex	1	0.028	4.23	3.43	**0.001**	1	0.022	4.03	3.58	**0.001**
	locality	9	0.211	3.51	6.53	**0.001**	9	0.231	4.63	9.49	**0.001**
	Csize:sex	1	0.013	1.99	1.64	0.071	1	0.009	1.55	1.39	0.086
	Csize:locality	9	0.066	1.10	0.53	0.285	9	0.072	1.45	2.59	**0.005**
	sex:locality	5	0.058	1.76	2.22	**0.018**	5	0.027	0.99	0.06	0.463
	Csize:sex:locality	5	0.032	0.98	-0.01	0.478	5	0.025	0.91	-0.49	0.691
P. sicula	Csize	1	0.121	11.52	5.08	**0.001**	1	0.196	19.92	6.93	**0.001**
	sex	1	0.046	4.38	3.25	**0.002**	1	0.067	6.80	4.95	**0.001**
	locality	5	0.269	5.15	6.37	**0.001**	5	0.192	3.90	7.19	**0.001**
	Csize:sex	1	0.023	2.22	1.94	**0.043**	1	0.022	2.24	2.47	**0.007**
	Csize:locality	5	0.061	1.17	0.77	0.225	5	0.049	1.01	0.09	0.461
	sex:locality	5	0.052	1.00	0.02	0.470	5	0.076	1.53	2.41	**0.007**
	Csize:sex:locality	5	0.061	1.18	0.68	0.249	5	0.052	1.06	0.37	0.368

Table 4: Results of the multiple regressions between bite force (BF), the proportion of plants (PLANT), the proportion of hard prey items (HARD), the sexual dimorphism in head dimensions (SDhead) and the PCSA of the 5 muscle groups (DM: jaw opener, ADD: external adductors, PSEU: pseudotemporalis, PTG: pterygoids, CONST: constrictor dorsalis muscles). s: slope, β: standardized coefficient, R^2: coefficient of determination, *P*: p-value. Bold values indicate retained models. Values in blue and red indicate a negative and a positive correlation, respectively.

			Females				Males			
			Raw		Residuals		Raw		Residuals	
No correction for phylogeny	BF	Model	***P* < 0.001**		***P* = 0.001**		***P* = 0.04**		*P* = 0.084	
			R^2 = 0.854		**R^2 = 0.71**		**R^2 = 0.3**		R^2 = 0.212	
		DM								
		ADD	s = 2.838	β = 0.35	s = 3.06	β = 0.16	s = 1.629	β = 0.16		
		PSEU	s = -1.384	β = -0.20	s = -1.212	β = -0.07				
		PTG					s = -1.231	β = -0.13		
		CONST								
	PLANT	Model	***P* = 0.012**		***P* = 0.013**		***P* = 0.013**		***P* = 0.037**	
			R^2 = 0.541		**R^2 = 0.422**		**R^2 = 0.53**		**R^2 = 0.423**	
		DM					s = 2.635	β = 0.23	s = 2.524	β = 0.16
		ADD					s = 7.716	β = 0.76	s = 7.479	β = 0.40
		PSEU	s = 7.550	β = 1.07	s = 3.966	β = 0.24				
		PTG	s = -6.912	β = -0.88			s = -6.656	β = -0.70	s = -6.713	β = -0.38
		CONST					s = -2.644	β = -0.23	s = -2.578	β = -0.19
	HARD	Model	***P* = 0.033**		***P* = 0.030**		*P* = 0.113		***P* = 0.008**	
			R^2 = 0.425		**R^2 = 0.439**		R^2 = 0.175		**R^2 = 0.574**	
		DM								
		ADD	s = -4.607	β = -0.56	s = -4.455	β = -0.23			s = -3.955	β = -0.21
		PSEU							s = 2.729	β = 0.15
		PTG	s = 4.167	β = 0.53	s = 3.592	β = 0.15			s = 3.485	β = 0.20
		CONST							s = -0.703	β = -0.05
	SDhead	Model	***P* = 0.004**		*P* = 0.198		***P* = 0.040**		*P* = 0.150	
			R^2 = 0.540		R^2 = 0.077		**R^2 = 0.289**		R^2 = 0.138	
		DM					s = 0.991	β = 0.09		
		ADD								
		PSEU					s = -1.311	β = -0.14		
		PTG	s = -1.149	β = -0.15						
		CONST								
With correction for phylogeny	BF	Model	**σ^2 <0.001**		**σ^2 = 0.001**		**σ^2 = 0.001**		**σ^2 = 0.001**	
		DM								
		ADD	s = 3.451	*P* = 0.003	s = 3.493	*P* = 0.003	s = 2.568	*P* = 0.013	s = 3.193	*P* = 0.007
		PSEU	s = -2.065	*P* = 0.023	s = -2.097	*P* = 0.024				
		PTG					s = -1.934	*P* = 0.029	s = -2.009	*P* = 0.020
		CONST								
	PLANT	Model	**σ^2 = 0.011**		σ^2 = 0.021		**σ^2 = 0.008**		**σ^2 = 0.009**	
		DM					s = 1.768	*P* = 0.052	s = 1.395	*P* = 0.132
		ADD					s = 7.384	*P* = 0.015	s = 5.595	*P* = 0.049
		PSEU	s = 5.709	*P* = 0.043						
		PTG	s = -3.333	*P* = 0.156			s = -5.523	*P* = 0.027	s = -4.222	*P* = 0.101
		CONST					s = -2.771	*P* = 0.011	s = -2.797	*P* = 0.017
	HARD	Model	**σ^2 = 0.003**		**σ^2 = 0.003**		**σ^2 = 0.008**		**σ^2 = 0.002**	
		DM	s = -1.891	*P* = 0.025	s = -1.852	*P* = 0.037			s = -0.964	*P* = 0.066
		ADD	s = -2.840	*P* = 0.139	s = -2.752	*P* = 0.104	s = -2.506	*P* = 0.092	s = -4.177	*P* = 0.003
		PSEU					s = 3.245	*P* = 0.039	s = 4.345	*P* = 0.002
		PTG	s = 3.920	*P* = 0.040	s = 3.951	*P* = 0.042			s = 2.599	*P* = 0.004
		CONST								
	SDhead	Model	**σ^2 = 0.003**		**σ^2 = 0.002**		**σ^2 = 0.001**		**σ^2 = 0.002**	
		DM								
		ADD	s = -2.104	*P* = 0.129	s = -2.408	*P* = 0.144	s = -1.736	*P* = 0.098	s = -1.985	*P* = 0.079
		PSEU			s = 1.724	*P* = 0.169			s = 1.361	*P* = 0.094
		PTG					s = 0.977	*P* = 0.083	s = 1.049	*P* = 0.222
		CONST								

667 **Table 5**: Results of the Procrustes ANOVAs with permutation testing for the effect of allometry on
668 observed variation in mandible and skull shape (*P:* p-value, F: F-statistic, R^2: coefficient of
669 determination, Z: effect sizes based on F distribution). Bold values indicate statistically significant
670 influence of allometry ($P < 0.05$).

	Without correction for phylogeny				**With correction for phylogeny**			
	Skull		Mandible		Skull		Mandible	
Females	***P* = 0.001 ***	F = 8.965	***P* = 0.001 ***	F = 12.732	*P* = 0.453	F = 0.879	***P* = 0.030 ***	F = 2.728
	R^2 = 0.134	Z = 4.362	R^2 = 0.180	Z = 6.058	R^2 = 0.081	Z = 0.076	R^2 = 0.214	Z = 1.793
Males	***P* = 0.001 ***	F = 8.237	***P* = 0.001 ***	F = 5.919	*P* = 0.415	F = 0.952	*P* = 0.281	F = 1.209
	R^2 = 0.097	Z = 4.796	R^2 = 0.071	Z = 4.671	R^2 = 0.064	Z = 0.154	R^2 = 0.079	Z = 0.643
P. melisellensis	***P* = 0.001 ***	F = 29.085	***P* = 0.001 ***	F = 40.809	*P* = 0.291	F = 1.118	*P* = 0.178	F = 1.492
	R^2 = 0.272	Z = 6.229	R^2 = 0.343	Z = 6.678	R^2 = 0.121	Z = 0.238	R^2 = 0.094	Z = 0.847
P. sicula	***P* = 0.001 ***	F = 7.810	***P* = 0.001 ***	F = 13.805	*P* = 0.624	F = 0.636	*P* = 0.744	F = 0.524
	R^2 = 0.121	Z = 4.380	R^2 = 0.195	Z = 6.159	R^2 = 0.089	Z = -0.162	R^2 = 0.071	Z = -0.289
Females *P. melisellensis*	***P* = 0.004 ***	F = 4.648	***P* = 0.017 ***	F = 2.327	*P* = 0.846	F = 0.448	*P* = 0.625	F = 0.719
	R^2 = 0.142	Z = 3.153	R^2 = 0.077	Z = 2.195	R^2 = 0.101	Z = -0.922	R^2 = 0.152	Z = -0.293
Males *P. melisellensis*	***P* = 0.001 ***	F = 5.809	***P* = 0.001 ***	F = 4.663	*P* = 0.213	F = 1.413	*P* = 0.604	F = 0.729
	R^2 = 0.108	Z = 4.088	R^2 = 0.089	Z = 3.783	R^2 = 0.150	Z = 0.808	R^2 = 0.083	Z = -0.273
Females *P. sicula*	*P* = 0.199	F = 1.419	***P* = 0.001 ***	F = 2.901	*P* = 0.588	F = 0.575	*P* = 0.098	F = 3.009
	R^2 = 0.048	Z = 0.838	R^2 = 0.094	Z = 2.916	R^2 = 0.126	Z = -0.396	R^2 = 0.429	Z = 1.565
Males *P. sicula*	***P* = 0.040 ***	F = 2.292	***P* = 0.001 ***	F = 4.731	*P* = 0.911	F = 0.385	*P* = 0.186	F = 1.377
	R^2 = 0.078	Z = 1.916	R^2 = 0.149	Z = 4.286	R^2 = 0.088	Z = -1.218	R^2 = 0.256	Z = 0.623

671

Table 6: Results of the two-block partial least-squares analyses (2b-PLS) between bite force (BF), muscular data (muscle PCSA, mass and fiber length), ecology (proportion of plants and hard items consumed, and the level of intraspecific competition) and 3D morphology at the population level. Also listed are the results of analyses using residual data (r) against raw shapes and allometry-free shapes (AF). P: P-value, rPLS: coefficient of covariation, % covar: percentage of covariance explained by the PLS axis considered. Bold values are statistically significant (P < 0.05) and associated results are highlighted in grey.

		Without correction for phylogeny				With correction for phylogeny				
		Female		Male		Female		Male		
		Skull	Mandible	Skull	Mandible	Skull	Mandible	Skull	Mandible	
BF	*P*	**0.005**	**0.001**	0.131	0.351	**0.036**	0.445	0.398	0.465	Raw shape
	rPLS	0.831	0.866	0.637	0.655	0.756	0.616	0.598	0.590	
	%covar	100	100	100	100	-	-	-	-	
Musculature	*P*	**0.003**	**0.002**	**0.011**	0.067	**0.001**	**0.045**	**0.042**	0.080	
	rPLS	0.855	0.905	0.782	0.727	0.946	0.827	0.771	0.739	
	%covar	96.560	96.878	87.127	88.219	-	-	-	-	
Ecology	*P*	**0.017**	**0.013**	**0.019**	**0.011**	0.281	0.422	**0.037**	**0.014**	
	rPLS	0.790	0.815	0.769	0.868	0.661	0.664	0.782	0.831	
	%covar	90.397	90.310	68.359	74.995	-	-	-	-	
rBF	*P*	0.622	0.768	0.306	0.291	0.089	0.378	0.320	0.506	
	rPLS	0.538	0.599	0.626	0.649	0.723	0.644	0.623	0.579	
	%covar	100	100	100	100	-	-	-	-	
rMusculature	*P*	0.393	0.764	**0.036**	0.195	**0.001**	0.061	**0.008**	0.063	
	rPLS	0.708	0.771	0.874	0.833	0.941	0.844	0.841	0.787	
	%covar	63.232	53.887	61.496	60.359	-	-	-	-	
rBF	*P*	0.411	0.414	0.180	0.145	0.399	0.446	0.184	0.293	AF shape
	rPLS	0.749	0.689	0.748	0.649	0.629	0.623	0.679	0.705	
	%covar	100	100	100	100	-	-	-	-	
rMusculature	*P*	**0.005**	0.119	**0.001**	**0.043**	**0.001**	**0.027**	**0.006**	**0.048**	
	rPLS	0.904	0.859	0.877	0.844	0.963	0.883	0.858	0.827	
	%covar	63.013	54.795	66.935	65.803	-	-	-	-	
Ecology	*P*	0.649	0.213	**0.001**	**0.001**	0.192	0.351	**0.023**	**0.011**	
	rPLS	0.898	0.793	0.892	0.845	0.729	0.681	0.810	0.875	
	%covar	61.512	86.521	42.825	76.967	-	-	-	-	

Table 7: Comparisons of the covariation patterns at the different levels of biological integration (BF: bite force, res: residual, F: females, M: males, meli: *P. melisellensis*, sicula: *P. sicula, P*: p-value, rPLS: coefficient of covariation, AF shape: allometry-free shape). Bold values indicate a significant difference between the compared rPLS.

					Skull				Mandible				
					P	rPLS 1	rPLS 2	Z-score	*P*	rPLS 1	rPLS 2	Z-score	
BF	Between sexes	F. meli	x	M. meli	0.219	0.91	0.673	1.227	0.274	0.853	0.617	1.093	Raw shape
		F. sicula	x	M. sicula	0.832	0.75	0.749	0.212	**0.017**	**0.918**	**0.605**	**2.390**	
	Between species	F. meli	x	F. sicula	0.504	0.91	0.75	0.668	0.856	0.853	0.918	0.182	
		M. meli	x	M. sicula	0.884	0.673	0.749	0.146	0.549	0.617	0.605	0.598	
	Intra vs. Interspecific	F. meli	x	all females	0.259	0.91	0.831	1.128	0.094	0.853	0.867	1.677	
		F. sicula	x	all females	0.115	0.75	0.831	1.576	0.114	0.918	0.867	1.580	
		M. meli	x	all males	0.522	0.673	0.637	0.641	0.405	0.617	0.655	0.833	
		M. sicula	x	all males	0.664	0.749	0.637	0.435	0.088	0.605	0.655	1.709	
Musculature	Between sexes	F. meli	x	M. meli	0.125	0.836	0.934	1.534	0.933	0.828	0.732	0.084	
		F. sicula	x	M. sicula	0.459	0.813	0.946	0.739	0.271	0.978	0.902	1.101	
	Between species	F. meli	x	F. sicula	0.999	0.836	0.813	0.001	0.173	0.828	0.978	1.363	
		M. meli	x	M. sicula	0.456	0.934	0.946	0.746	0.809	0.732	0.902	0.241	
	Intra vs. Interspecific	F. meli	x	all females	0.082	0.836	0.855	1.739	**0.024**	**0.828**	**0.905**	**2.263**	
		F. sicula	x	all females	0.104	0.813	0.855	1.627	0.176	0.978	0.905	1.353	
		M. meli	x	all males	0.776	0.934	0.782	0.284	0.677	0.732	0.727	0.417	
		M. sicula	x	all males	0.662	0.946	0.782	0.437	0.785	0.902	0.727	0.272	
Ecology	Between sexes	F. meli	x	M. meli	0.182	0.869	0.956	1.333	**0.007**	**0.692**	**0.902**	**2.702**	
		F. sicula	x	M. sicula	0.548	0.837	0.915	0.601	0.966	0.909	0.855	0.041	
	Between species	F. meli	x	F. sicula	0.993	0.869	0.837	0.009	**0.046**	**0.692**	**0.909**	**1.994**	
		M. meli	x	M. sicula	0.535	0.956	0.915	0.619	0.198	0.902	0.855	1.288	
	Intra vs. Interspecific	F. meli	x	all females	0.335	0.869	0.790	0.964	**0.008**	**0.692**	**0.815**	**2.662**	
		F. sicula	x	all females	0.355	0.837	0.790	0.925	0.168	0.909	0.815	1.377	
		M. meli	x	all males	0.465	0.956	0.770	0.731	0.984	0.902	0.868	0.024	
		M. sicula	x	all males	0.959	0.915	0.770	0.051	0.141	0.855	0.868	1.474	
resBF	Between sexes	F. meli	x	M. meli	0.539	0.822	0.661	0.614	0.479	0.805	0.620	0.706	
		F. sicula	x	M. sicula	0.659	0.728	0.681	0.440	**0.044**	**0.887**	**0.670**	**2.005**	
	Between species	F. meli	x	F. sicula	0.748	0.822	0.728	0.321	0.509	0.805	0.887	0.659	
		M. meli	x	M. sicula	0.818	0.661	0.681	0.229	0.888	0.620	0.670	0.140	
	Intra vs. Interspecific	F. meli	x	all females	0.687	0.822	0.538	0.402	0.971	0.805	0.599	0.036	
		F. sicula	x	all females	0.917	0.728	0.538	0.105	0.631	0.887	0.599	0.480	
		M. meli	x	all males	0.522	0.661	0.626	0.640	0.439	0.620	0.650	0.774	
		M. sicula	x	all males	0.793	0.681	0.626	0.428	0.281	0.670	0.650	1.079	
resMusculature	Between sexes	F. meli	x	M. meli	0.303	0.869	0.904	1.030	0.311	0.963	0.922	1.013	
		F. sicula	x	M. sicula	0.809	0.915	0.924	0.241	0.503	0.844	0.761	0.669	
	Between species	F. meli	x	F. sicula	0.347	0.869	0.915	0.939	0.172	0.963	0.844	1.367	
		M. meli	x	M. sicula	0.767	0.904	0.924	0.297	**0.008**	**0.922**	**0.761**	**2.637**	
	Intra vs. Interspecific	F. meli	x	all females	0.887	0.869	0.708	0.142	0.783	0.963	0.771	0.275	
		F. sicula	x	all females	0.328	0.915	0.708	0.978	0.379	0.844	0.771	0.879	
		M. meli	x	all males	0.622	0.904	0.874	0.492	0.502	0.922	0.833	0.671	
		M. sicula	x	all males	0.436	0.924	0.874	0.778	**0.035**	**0.761**	**0.833**	**2.104**	
resBF	Between sexes	F. meli	x	M. meli	0.914	0.866	0.712	0.108	0.899	0.793	0.798	0.127	AF shape
		F. sicula	x	M. sicula	0.790	0.715	0.781	0.266	0.909	0.877	0.863	0.113	
	Between species	F. meli	x	F. sicula	0.747	0.866	0.715	0.323	0.955	0.793	0.877	0.056	
		M. meli	x	M. sicula	0.601	0.712	0.781	0.523	0.861	0.798	0.863	0.175	
	Intra vs. Interspecific	F. meli	x	all females	0.892	0.866	0.749	0.136	0.822	0.793	0.689	0.224	
		F. sicula	x	all females	0.621	0.715	0.749	0.495	0.811	0.877	0.689	0.239	
		M. meli	x	all males	0.524	0.712	0.748	0.637	0.851	0.798	0.684	0.188	
		M. sicula	x	all males	0.191	0.781	0.748	1.308	0.660	0.863	0.684	0.439	
resMusculature	Between sexes	F. meli	x	M. meli	0.276	0.951	0.918	1.088	0.754	0.956	0.924	0.314	
		F. sicula	x	M. sicula	0.900	0.878	0.973	0.126	0.773	0.910	0.866	0.289	
	Between species	F. meli	x	F. sicula	0.703	0.951	0.878	0.381	0.224	0.956	0.910	1.216	
		M. meli	x	M. sicula	0.407	0.918	0.973	0.829	0.256	0.924	0.866	1.134	
	Intra vs. Interspecific	F. meli	x	all females	0.582	0.951	0.904	0.550	0.439	0.956	0.859	0.773	
		F. sicula	x	all females	0.939	0.878	0.904	0.077	0.668	0.910	0.859	0.429	
		M. meli	x	all males	0.964	0.918	0.877	0.046	0.799	0.924	0.844	0.254	
		M. sicula	x	all males	0.342	0.973	0.877	0.950	0.177	0.866	0.844	1.349	
Ecology	Between sexes	F. meli	x	M. meli	**0.029**	**0.828**	**0.959**	**2.177**	**0.009**	**0.665**	**0.966**	**2.621**	
		F. sicula	x	M. sicula	0.908	0.799	0.861	0.115	0.322	0.940	0.824	0.991	
	Between species	F. meli	x	F. sicula	0.617	0.828	0.799	0.500	0.055	0.665	0.940	1.921	
		M. meli	x	M. sicula	0.084	0.959	0.861	1.729	0.054	0.966	0.824	1.928	
	Intra vs. Interspecific	F. meli	x	all females	**0.049**	**0.828**	**0.898**	**1.966**	0.075	0.665	0.793	1.783	

F. sicula	x	all females	0.254	0.799	0.898	1.141	0.812	0.940	0.793	0.237
M. meli	x	all males	0.604	0.959	0.843	0.519	0.932	0.966	0.845	0.085
M. sicula	x	all males	0.175	0.861	0.843	1.354	0.071	0.824	0.845	1.804

694

Figure legends:

Figure 1: illustration of the landmarks used to quantify the shape of the cranium. Large blue circles represent anatomical landmarks and small orange circles represent sliding landmarks on curves (a-b-c-d: dorsal, left lateral, ventral, caudal views of the skull).

Figure 2: illustration of the landmarks used to quantify the shape of the mandible. Large blue circles represent anatomical landmarks and small orange circles represent sliding landmarks on curves (a-b-c: left lateral and medial views of the left mandible, and dorsal focus on the retro-articular process).

Figure 3: results of the 2b-PLS analysis exploring the covariation between ecology and skull shape in females (circles: *P. melisellensis* populations, squares: *P. sicula* populations). Red shapes (and red lollipops) represent the theoretical deformations associated with the positive side of the covariation axis (blue shapes: negative side). The histogram gives the contributions of each variable to the axis of covariation. Note the differences in the adductor chamber size, snout length, and the curvature of the quadrate.

Figure 4: results of the 2b-PLS analysis exploring the covariation between ecology and allometry-free mandible shape in males (circles: *P. melisellensis* populations, squares: *P. sicula* populations). Red shapes (and red lollipops) represent the theoretical deformations associated with the positive side of the axis of covariation (blue shapes: negative side). The histogram gives the contributions of each variable to the axis of covariation. Note the differences in overall mandible robustness, the thickness of the coronoid process, and the lateral area for muscle insertion.

Figure 5: comparison of the results of the 2b-PLS analysis exploring the covariation between muscle architecture and skull shape in all males (A, C, E) (circles: *P. melisellensis*, squares: *P. sicula*), and in males of *P. melisellensis* populations only (B, D, F). Red lollipops represent the theoretical deformations associated with the positive side of the axis of covariation (blue lollipops: negative side). The histograms give the contributions of each muscular variable to the axis of covariation. Note the differences in the adductor chamber size, snout length, and the curvature of the quadrate and of the pterygoid bone.

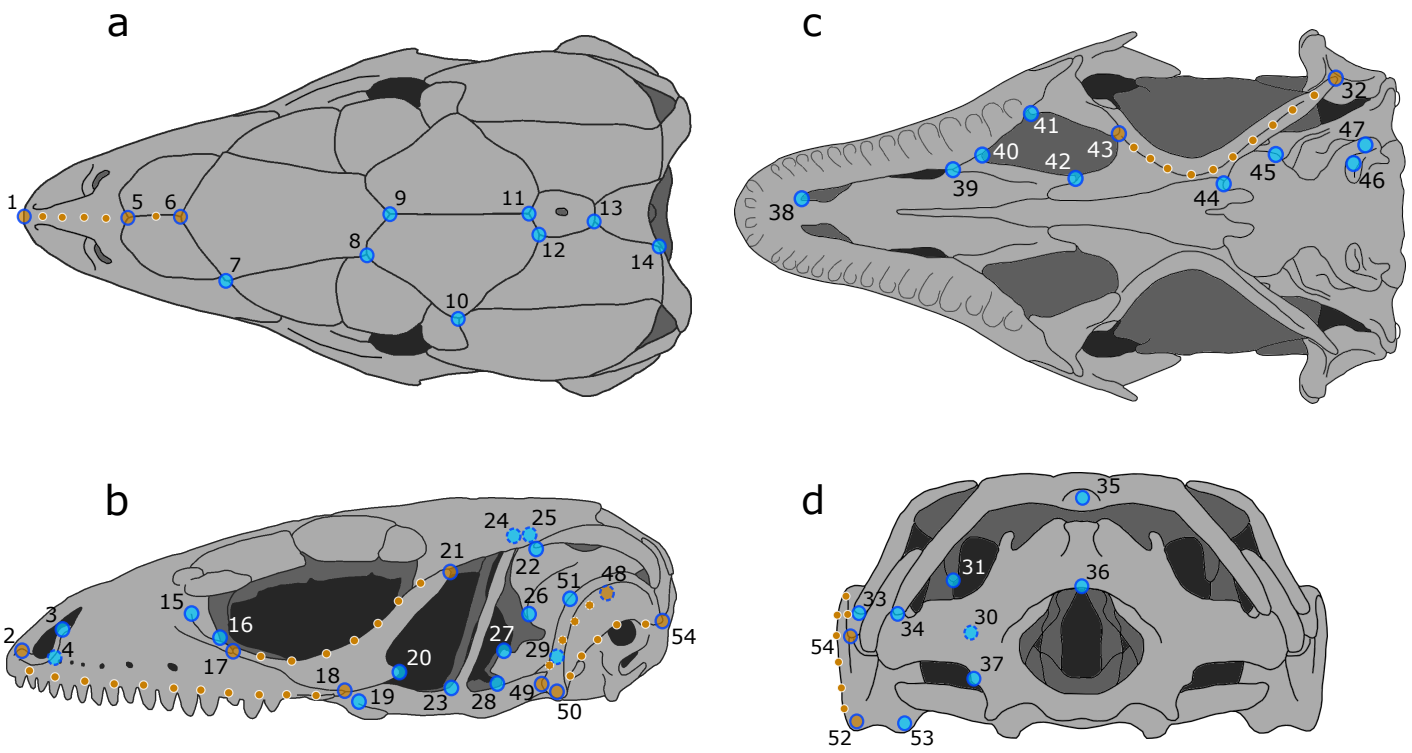
a
1
5
6
9
11
13
8
12
14
7
10
c
32
41
47
40
42
43
45
46
39
44
38
b
24
25
21
22
51
48
15
26
3
16
27
54
2
29
4
20
17
18
19
23
28
49
50
d
35
31
36
33
34
30
54
37
52
53

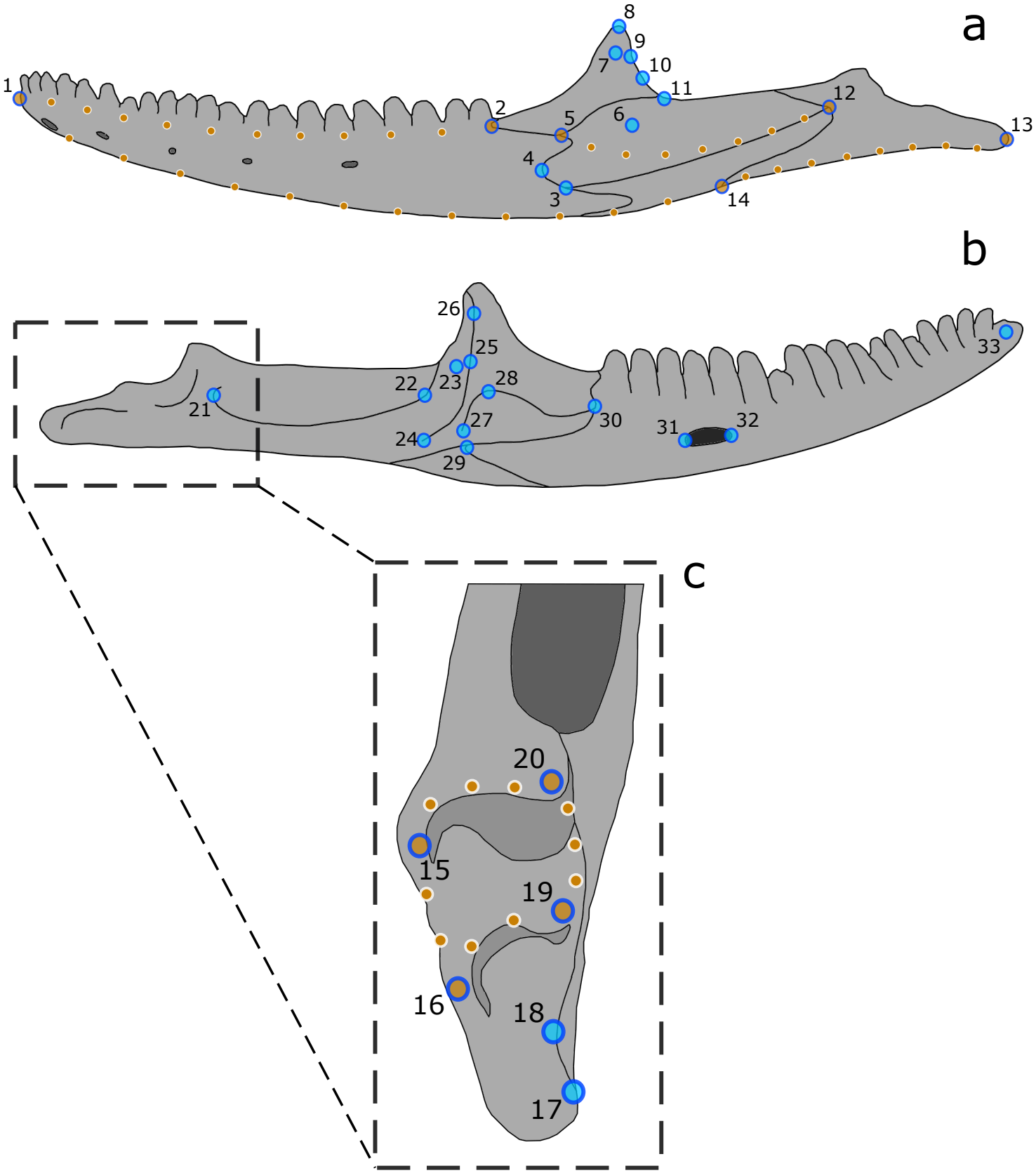
a
1
2
3
4
5
6
7
8
9
10
11
12
13
14
b
21
22
23
24
25
26
27
28
29
30
31
32
33
c
15
16
17
18
19
20

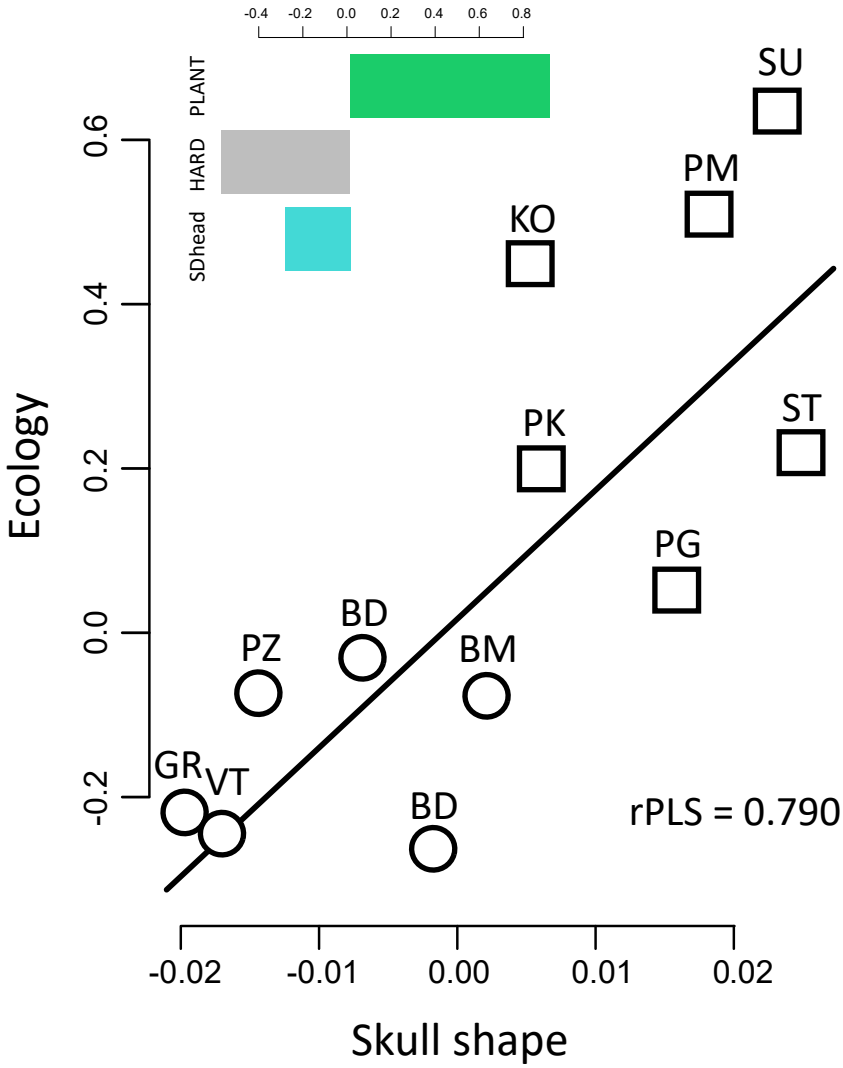
-0.4 -0.2 0.0 0.2 0.4 0.6 0.8
PLANT
HARD
SDhead
SU
PM
KO
PK
ST
PG
BD
PZ
BM
GR
VT
BD
rPLS = 0.790
Ecology
0.6
0.4
0.2
0.0
-0.2
-0.02
-0.01
0.00
0.01
0.02
Skull shape

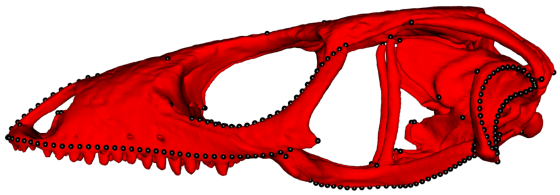

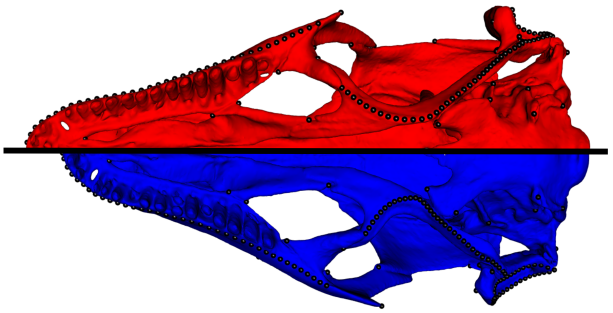

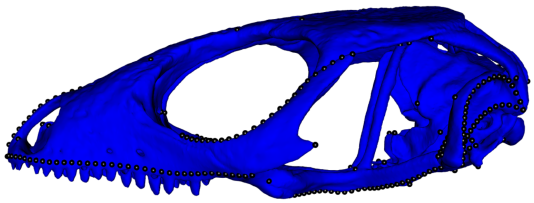

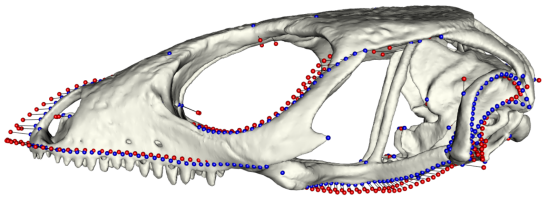

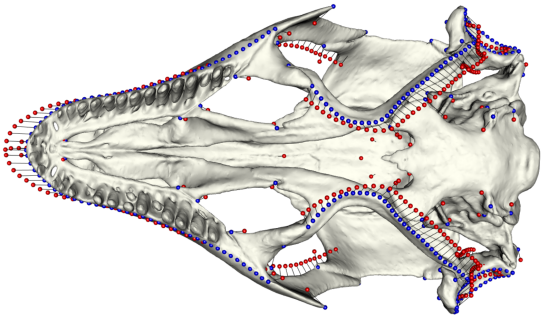

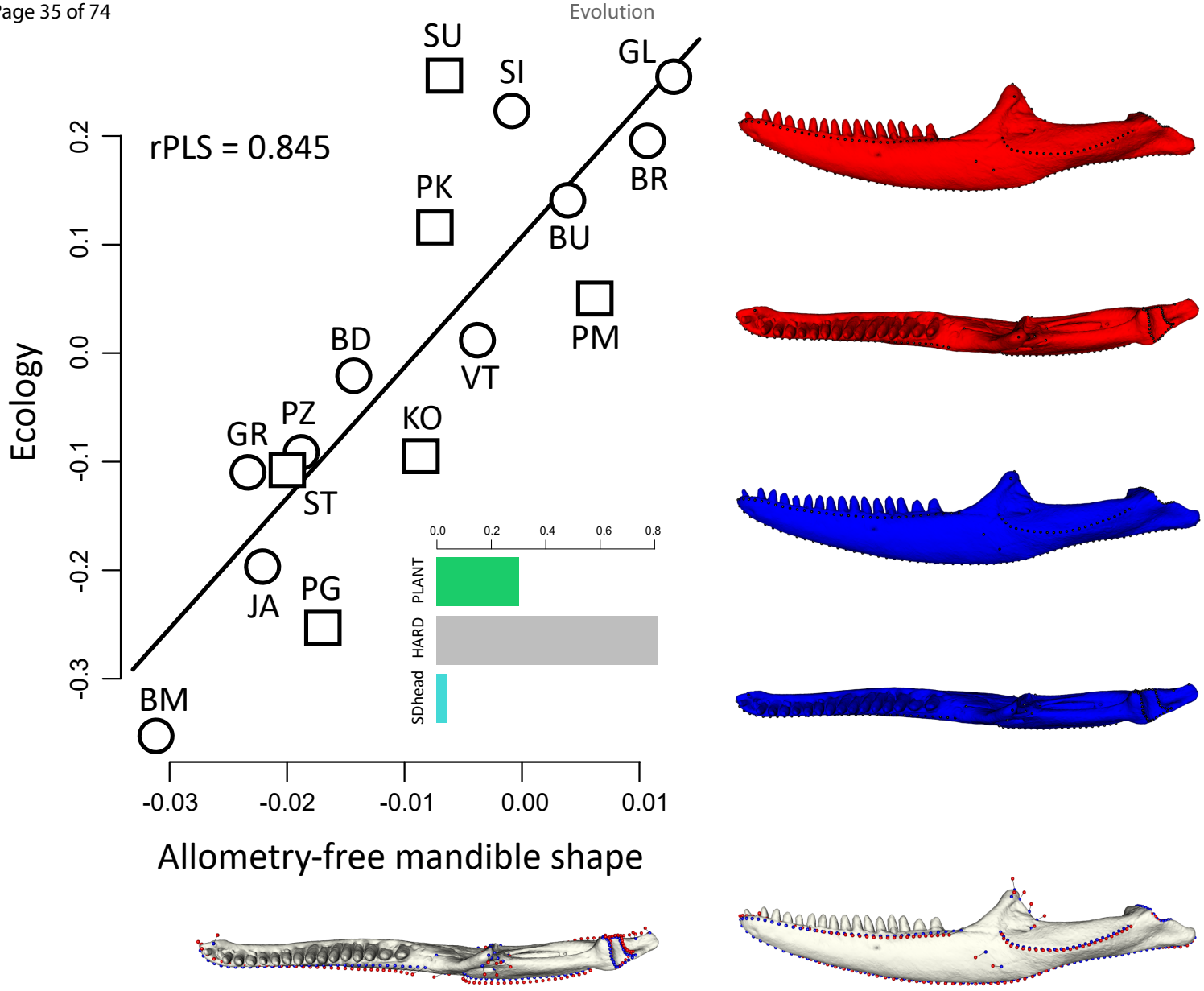
rPLS = 0.845
Ecology
Allometry-free mandible shape
SU
SI
GL
BR
PK
BU
PM
BD
VT
PZ
KO
GR
ST
JA
PG
BM
PLANT
HARD
SDhead
0.0
0.2
0.4
0.6
0.8
-0.3
-0.2
-0.1
0.0
0.1
0.2
-0.03
-0.02
-0.01
0.00
0.01

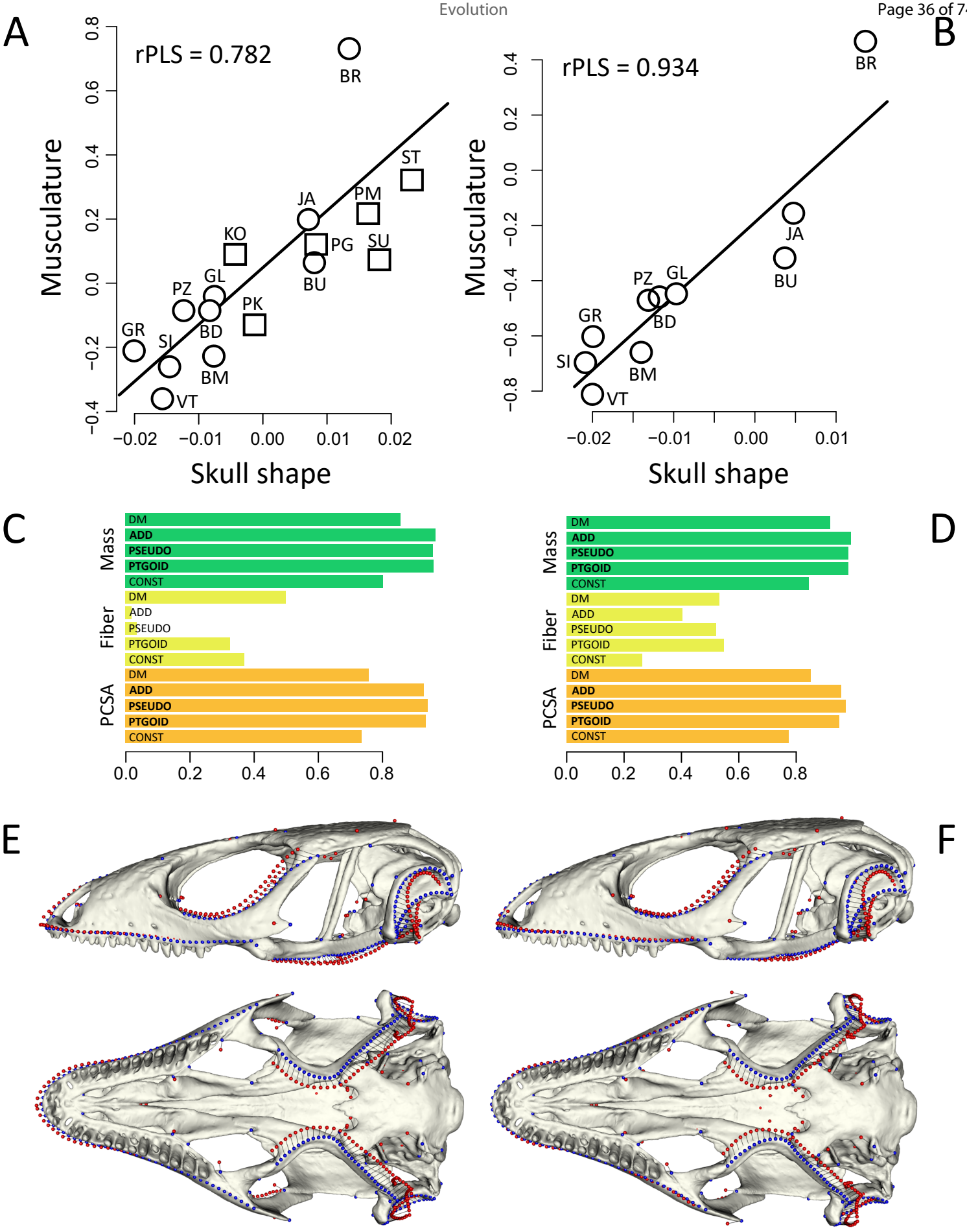
A
rPLS = 0.782
Musculature
Skull shape
BR
ST
PM
JA
KO
PG
SU
BU
GL
PZ
PK
BD
GR
SI
BM
VT
B
rPLS = 0.934
Musculature
Skull shape
BR
JA
BU
PZ
GL
BD
GR
SI
BM
VT
C
D
Mass
Fiber
PCSA
DM
ADD
PSEUDO
PTGOID
CONST
0.0
0.2
0.4
0.6
0.8
E
F

Supplementary Information 1: Distribution of all the individuals included in the present study in the morphospace based on skull shape data. BD: Veli Budikovać, BM: Mali Barjak, Br: Brusnik, Bu: Veli Barjak, GL: Glavat, GR: Greben, J: Jabuka, Ko: Kopište, PG: Mala Palagruža, PK: Pod Kopište, PM: Pod Mrčaru, PZ: Mali Parzanj, Si: Sinj, St: Split, Su: Susać, T: Veli Tajana.

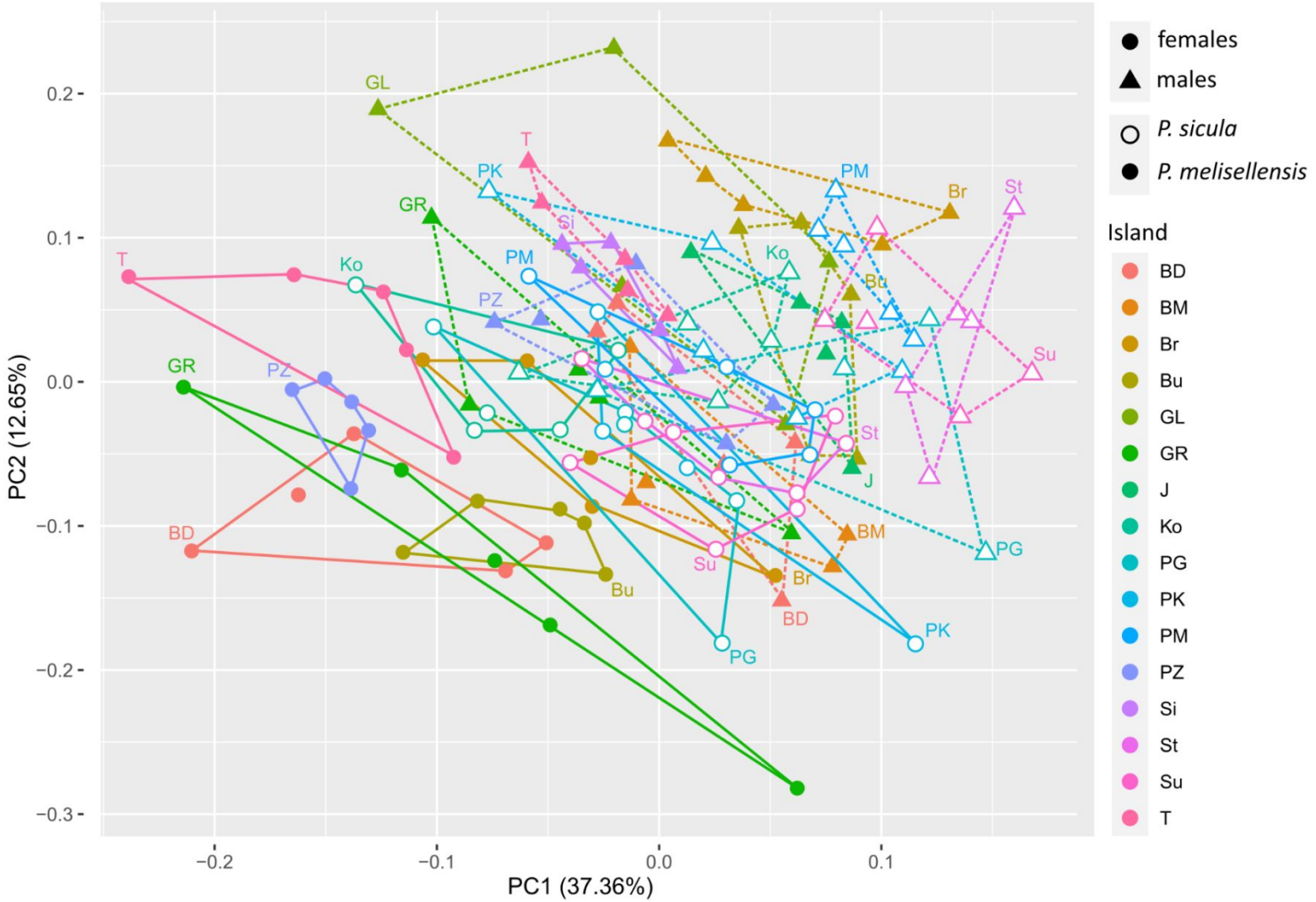

Supplementary Information 2: Interspecific comparisons of the allometric trajectories between the PCSA of the main jaw muscle groups and skull centroid size (Csize). Represented are female individuals of *P. sicula* (in red) and of *P. melisellensis* (in black). Note that although significant, differences in allometric slopes between species are slight.

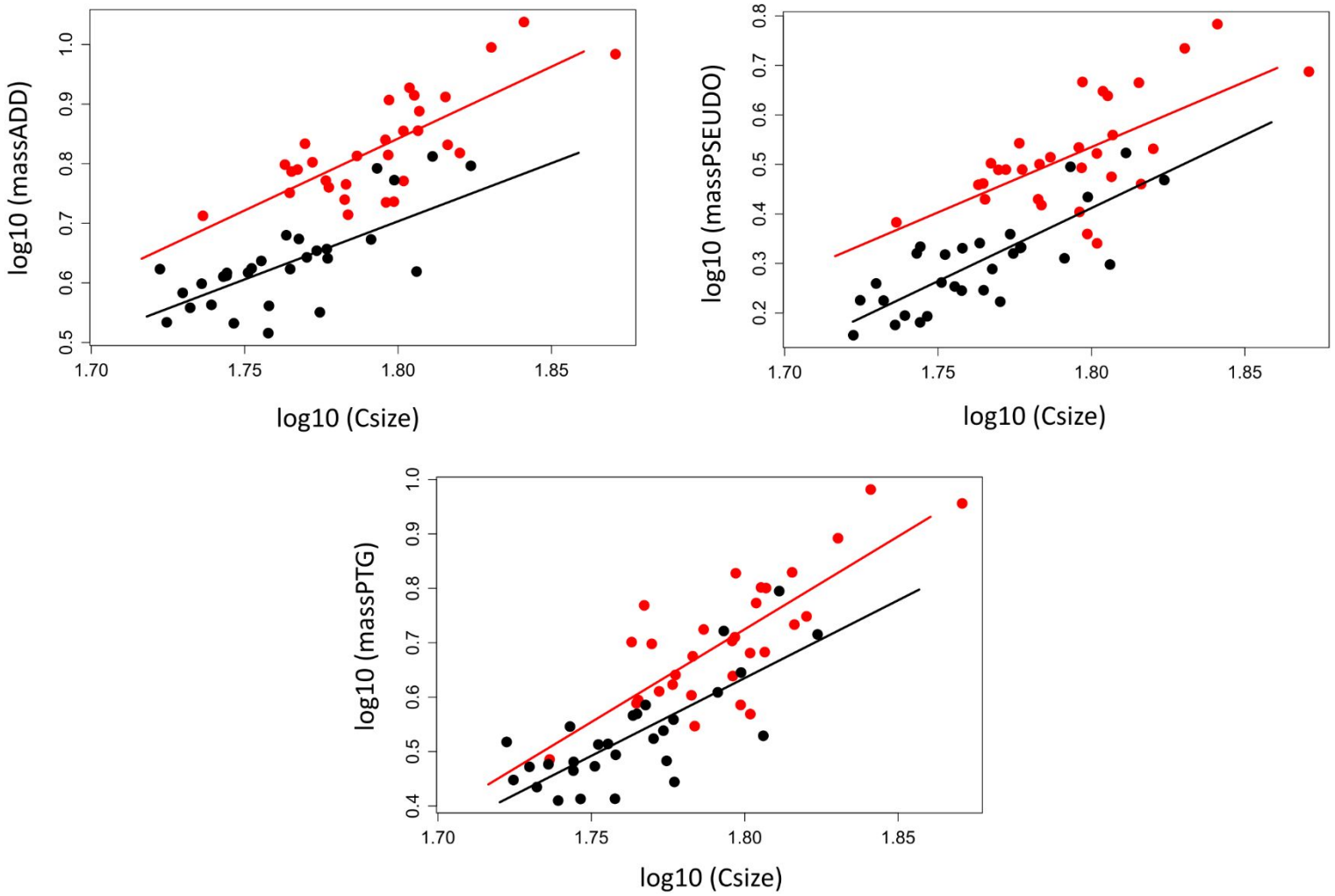

Supplementary Information 3: Contributions of the variables within each block to the axes of covariation resulting from the two-block partial least squares analyses (2b-pls). DM: depressor mandibulae, ADD: external adductors, PSEUDO: pseudotemporalis muscles, PTGOID: pterygoids, CONST: constrictor dorsalis, mass: muscle mass, fiber: fiber length, pcsa: Physiological Cross-Sectional Area of the muscle, AF shape: shape corrected for the allometry.

		Without correction for phylogeny				With correction for phylogeny				
		Females		Males		Females		Males		
		Skull	Mandible	Skull	Mandible	Skull	Mandible	Skull	Mandible	
Musculature	massDM	0.890	0.886	0.870		0.056	0.401	-0.311		vs. Raw shape
	massADD	0.956	0.965	0.981		-0.174	0.267	-0.233		
	massPSEUDO	0.976	0.982	0.973		-0.106	0.268	-0.287		
	massPTGOID	0.977	0.981	0.974		-0.197	0.387	-0.354		
	massCONST	0.797	0.785	0.815		0.576	0.374	-0.001		
	fiberDM	0.782	0.790	0.508		-0.099	0.037	-0.018		
	fiberADD	-0.165	-0.153	0.018		-0.169	0.077	0.141		
	fiberPSEUDO	-0.121	-0.102	0.035		-0.256	0.057	0.075		
	fiberPTGOID	0.385	0.399	0.331		-0.224	0.088	0.177		
	fiberCONST	0.543	0.549	0.376		-0.107	0.052	-0.072		
	pcsaDM	0.814	0.807	0.770		0.146	0.361	-0.293		
	pcsaADD	0.963	0.966	0.944		0.014	0.192	-0.365		
	pcsaPSEUDO	0.973	0.973	0.956		0.121	0.209	-0.345		
	pcsaPTGOID	0.982	0.983	0.949		0.013	0.288	-0.486		
	pcsaCONST	0.806	0.792	0.747		0.618	0.304	-0.067		
Ecology	Vplant	0.972	0.979	0.924	0.976			-0.604	0.123	
	Vhard	-0.548	-0.669	-0.290	-0.513			-0.782	-0.939	
	SDhead	-0.284	-0.241	0.665	-0.139			0.152	0.322	
resMusculature	massDM			0.267		0.058		-0.298		
	massADD			0.802		-0.164		-0.156		
	massPSEUDO			0.813		-0.093		-0.217		
	massPTGOID			0.794		-0.189		-0.266		
	massCONST			-0.045		0.574		0.096		
	fiberDM			-0.225		-0.096		0.037		
	fiberADD			-0.467		-0.175		0.219		
	fiberPSEUDO			-0.314		-0.261		0.133		
	fiberPTGOID			-0.501		-0.226		0.293		
	fiberCONST			-0.228		-0.107		-0.054		
	pcsaDM			0.350		0.145		-0.334		
	pcsaADD			0.939		0.028		-0.364		
	pcsaPSEUDO			0.949		0.139		-0.327		
	pcsaPTGOID			0.956		0.023		-0.502		
	pcsaCONST			0.259		0.619		-0.026		
resMusculature	massDM	-0.508		0.281	0.518	0.058	0.063	-0.32	-0.364	vs. AF shape
	massADD	0.599		0.815	0.956	-0.159	0.251	-0.151	-0.153	
	massPSEUDO	0.324		0.826	0.962	-0.073	0.261	-0.221	-0.268	
	massPTGOID	0.379		0.809	0.962	-0.185	0.315	-0.256	-0.269	
	massCONST	-0.813		-0.038	0.188	0.553	-0.539	0.093	0.062	
	fiberDM	0.476		-0.218	-0.007	-0.091	0.099	0.058	0.227	
	fiberADD	0.419		-0.445	0.012	-0.204	0.001	0.208	0.043	
	fiberPSEUDO	0.667		-0.291	0.133	-0.287	0.104	0.132	-0.001	
	fiberPTGOID	0.537		-0.481	-0.051	-0.238	0.132	0.283	0.181	
	fiberCONST	0.159		-0.221	-0.055	-0.109	0.102	-0.05	-0.025	
	pcsaDM	-0.572		0.360	0.489	0.139	-0.020	-0.378	-0.592	
	pcsaADD	-0.057		0.932	0.782	0.062	0.241	-0.346	-0.184	
	pcsaPSEUDO	-0.337		0.945	0.833	0.179	0.163	-0.331	-0.239	
	pcsaPTGOID	-0.282		0.959	0.925	0.034	0.176	-0.482	-0.408	

	pcsaCONST	-0.907		0.259	0.290	0.607	-0.557	-0.008	0.036
Ecology	Vplant			-0.237	0.299			-0.589	0.181
	Vhard			-0.789	0.806			-0.793	-0.939
	SDhead			0.283	-0.006			0.152	0.293

Supplementary Information 4: Results of the intraspecific two-block partial least-squares analyses (2b-PLS) between bite force (BF), muscular data (muscle PCSA and MASS), resource use (PLANT: proportion of plants, HARD: proportion of hard prey items in the diet) at the population level. Also listed are the results of analyses using residual data (r) against raw shapes and allometry-free shapes. P: P-value, rPLS: coefficient of covariation, % covar: percentage of covariance explained by the PLS axis considered. Bold values are statistically significant ($P < 0.05$).

		P. melisellensis				*P. sicula*				
		Females		Males		Females		Males		
		Skull	Mandible	Skull	Mandible	Skull	Mandible	Skull	Mandible	
BF	*P*	0.080	0.457	0.678	0.894	0.519	0.388	0.538	1.000	Raw shape
	rPLS	0.910	0.853	0.673	0.617	0.750	0.918	0.749	0.605	
	%covar	-	-	-	-	-	-	-	-	
Musculature	*P*	0.277	0.587	**0.002**	0.530	0.321	**0.033**	**0.029**	0.398	
	rPLS	0.836	0.828	0.934	0.732	0.813	0.978	0.946	0.902	
	%covar	-	-	-	-	-	-	-	-	
Ecology	*P*	0.240	0.981	**0.001**	**0.040**	0.235	0.306	0.096	0.409	
	rPLS	0.869	0.692	0.956	0.902	0.837	0.909	0.915	0.855	
	%covar	-	-	-	-	-	-	-	-	
rBF	*P*	0.419	0.650	0.735	0.888	0.547	0.290	0.785	0.985	
	rPLS	0.822	0.805	0.661	0.620	0.728	0.887	0.681	0.670	
	%covar	-	-	-	-	-	-	-	-	
rMusculature	*P*	0.320	0.084	**0.020**	**0.012**	**0.024**	0.747	0.078	0.918	
	rPLS	0.869	0.963	0.904	0.922	0.915	0.844	0.924	0.761	
	%covar	-	-	-	-	-	-	-		
rBF	*P*	0.380	0.509	0.391	0.622	0.473	0.504	0.679	0.451	AF shape
	rPLS	0.866	0.793	0.712	0.798	0.715	0.877	0.781	0.863	
	%covar	-	-	-	-	-	-	-	-	
rMusculature	*P*	0.086	**0.035**	**0.001**	0.072	0.104	0.415	**0.021**	0.551	
	rPLS	0.951	0.956	0.918	0.924	0.878	0.910	0.973	0.866	
	%covar	-	-	-	-	-	-	-	-	
Ecology	*P*	0.652	0.964	**0.001**	**0.002**	0.353	0.240	0.396	0.697	
	rPLS	0.828	0.665	0.959	0.966	0.799	0.940	0.861	0.824	
	%covar	-	-	-	-	-	-	-	-	

Supplementary Information 5: Results of the multiple regressions between bite force (BF), the proportion of plants (PLANT), the proportion of hard prey items (HARD), or the sexual dimorphism in head dimensions (SDh) on one hand, and the PCSA (Physiological Cross-Sectional Area), the mass and the mean fiber length of the 5 muscle groups (DM: jaw opener, ADD: external adductors, PSEU: pseudotemporalis, PTG: pterygoids, CONST: constrictor dorsalis muscles) on the other hand. s: slope, β: standardized coefficient, R^2: coefficient of determination, *P*: p-value. Bold values indicate retained models. Values in blue and red indicate a negative and a positive correlation, respectively.

			No correction for phylogeny								With correction for phylogeny							
			Females				Males				Females				Males			
			Raw		Residuals		Raw		Residuals		Raw		Residuals		Raw		Residuals	
Bite Force	PCSA	Model	**P < 0.001**		**P = 0.001**		**P = 0.04**		P = 0.084		**σ² <0.001**		**σ² = 0.001**		**σ² = 0.001**		**σ² = 0.001**	
			R² = 0.854		**R² = 0.71**		**R² = 0.3**		R² = 0.212									
		DM																
		ADD	s = 2.838	β = 0.35	s = 3.06	β = 0.16	s = 1.629	β = 0.16			s = 3.451	P = 0.003	s = 3.493	P = 0.003	s = 2.568	P = 0.013	s = 3.193	P = 0.007
		PSEU	s = -1.384	β = -0.20	s = -1.212	β = -0.07					s = -2.065	P = 0.023	s = -2.097	P = 0.024				
		PTG					s = -1.231	β = -0.13							s = -1.934	P = 0.029	s = -2.009	P = 0.020
		CONST																
	Mass	Model	**P <0.001**		**P = 0.01**		P = 0.212		P = 0.355		**σ² <0.001**		**σ² <0.001**		**σ² <0.001**		**σ² = 0.001**	
			R² = 0.812		**R² = 0.559**		R² = 0.09		R² = 0.016									
		DM															s = 1.604	P = 0.006
		ADD													s = 0.961	P = 0.033	s = 5.477	P = 0.002
		PSEU	s = 2.640	β = 0.36	s = 2.689	β = 0.15					s = 1.268	<0.001	s = 2.300	P = 0.029	s = -4.053	P = 0.016	s = -5.599	P = 0.001
		PTG	s = -1.466	β = -0.22	s = -1.333	β = -0.08												
		CONST													s = 1.312	P = 0.005		
	Fiber length	Model	**P = 0.001**		P = 0.054 .		**P = 0.027**		P = 0.057 .		**σ² = 0.001**		-		σ² = 0.002		-	
			R² = 0.7		R² = 0.359		**R² = 0.34**		R² = 0.256									
		DM	s = 4.204	β = 0.14														
		ADD	s = -1.039	β = -0.04			s = -2.175	β = -0.10										
		PSEU																
		PTG					s = 1.7	β = 0.08										
		CONST									s = 2.483	P = 0.010						
PLANT	PCSA	Model	**P = 0.012**		**P = 0.013**		**P = 0.013**		**P = 0.037**		**σ² = 0.011**		σ² = 0.021		**σ² = 0.008**		**σ² = 0.009**	
			R² = 0.541		**R² = 0.422**		**R² = 0.53**		**R² = 0.423**									
		DM					s = 2.635	β = 0.23	s = 2.524	β = 0.16					s = 1.768	P = 0.052	s = 1.395	P = 0.132
		ADD					s = 7.716	β = 0.76	s = 7.479	β = 0.40					s = 7.384	P = 0.015	s = 5.595	P = 0.049
		PSEU	s = 7.550	β = 1.07	s = 3.966	β = 0.24					s = 5.709	P = 0.043						
		PTG	s = -6.912	β = -0.88			s = -6.656	β = -0.70	s = -6.713	β = -0.38	s = -3.333	P = 0.156			s = -5.523	P = 0.027	s = -4.222	P = 0.101
		CONST					s = -2.644	β = -0.23	s = -2.578	β = -0.19					s = -2.771	P = 0.011	s = -2.797	P = 0.017
	Mass	Model	**P = 0.019**		**P = 0.033**		P = 0.208		P = 0.061 .		**σ² = 0.006**		**σ² = 0.006**		**σ² = 0.009**		**σ² = 0.010**	
			R² = 0.578		**R² = 0.428**		R² = 0.094		R² = 0.174									
		DM											s = -3.406	P = 0.093	s = 3.053	P = 0.026	s = 2.815	P = 0.049
		ADD	s = -15.265	β = -1.85	s = -13.382	β = -0.68					s = -13.131	P = 0.002	s = -12.304	P = 0.005				
		PSEU	s = 15.440	β = 2.13	s = 14.422	β = 0.81					s = 7.117	P = 0.047			s = -7.595	P = 0.035	s = -7.883	P = 0.047
		PTG									s = 4.850	P = 0.064	s = 10.253	P = 0.007	s = 4.669	P = 0.086	s = 4.748	P = 0.170
		CONST	s = -1.677	β =-0.18									s = 1.034	P = 0.118				
	Fiber length	Model	**P = 0.004**		**P = 0.003**		**P = 0.002**		**P = 0.009**		**σ² = 0.003**		**σ² = 0.010**		**σ² = 0.003**		**σ² = 0.005**	
			R² = 0.785		**R² = 0.668**		**R² = 0.606**		**R² = 0.512**									
		DM	s = -1.239	β = 0.19	s = 9.247	β = 0.16					s = 11.252	P = 0.012			s = -2.382	P = 0.044	s = -1.790	P = 0.110
		ADD	s = -7.048	β = -0.28									s = -6.326	P = 0.071			s = 3.912	P = 0.064
		PSEU					s = -7.905	β = -0.34	s = -8.290	β = -0.35	s = -8.854	P = 0.001			s = -9.162	P = 0.001	s = -9.000	P = 0.003
		PTG	s = 5.707	β = 0.23			s = 3.540	β = 0.17	s =3.949	β = 0.17	s = 6.344	P = 0.004	s = 6.767	P = 0.078	s = 3.688	P = 0.017		
		CONST	s = -7.860	β = -0.24	s = -15.008	β = -0.32	s = 3.042	β = 0.08	s = 3.654	β = 0.08	s = -7.162	P =0.079	s = -6.345	P = 0.137	s = 7.815	P = 0.001	s = 7.608	P = 0.002

		Model	**P = 0.033** **R² = 0.425**		**P = 0.030** **R² = 0.439**		P = 0.113 R² = 0.175		**P = 0.008** **R² = 0.574**		**σ² = 0.003**		**σ² = 0.003**		**σ² = 0.008**		**σ² = 0.002**	
		DM									s = -1.891	*P* = 0.025	s = -1.852	*P* = 0.037			s = -0.964	*P* = 0.066
	PCSA	ADD	s = -4.607	β = -0.56	s = -4.455	β = -0.23			s = -3.955	β = -0.21	s = -2.840	*P* = 0.139	s = -2.752	*P* = 0.104	s = -2.506	*P* = 0.092	s = -4.177	*P* = 0.003
		PSEU							s = 2.729	β = 0.15					s = 3.245	*P* = 0.039	s = 4.345	*P* = 0.002
		PTG	s = 4.167	β = 0.53	s = 3.592	β = 0.15			s = 3.485	β = 0.20	s = 3.920	*P* = 0.040	s = 3.951	*P* = 0.042			s = 2.599	*P* = 0.004
		CONST							s = -0.703	β = -0.05								
		Model	*P* = 0.374 R² = 0.082		*P* = 0.324 R² = 0.130		***P* = 0.006** **R² = 0.471**		***P* < 0.001** **R² = 0.692**		**σ² = 0.003**		**σ² = 0.003**		**σ² = 0.003**		**σ² = 0.003**	
		DM									s = -1.991	*P* = 0.015	s = -1.859	*P* = 0.057				
HARD	Mass	ADD					s = -10.662	β = -1.05	s = -5.573	β = -0.23					s = -4.718	*P* = 0.116	s = -4.637	*P* = 0.120
		PSEU					s = 9.583	β = 1.05	s = 7.604	β = 0.37					s = 10.667	*P* = 0.001	s = 10.336	*P* = 0.001
		PTG									s = 1.698	*P* = 0.009	s = 1.741	*P* = 0.011	s = -4.637	*P* = 0.090	s = -4.072	*P* = 0.157
		CONST							s = -1.108	β = -0.07					s = -1.788	*P* = 0.042	s = -1.686	*P* = 0.049
		Model	*P* = 0.095 R² = 0.426		***P* = 0.038** **R² = 0.568**		*P* = 0.194 R² = 0.104		*P* = 0.212 R² = 0.091		**σ² = 0.005**		**σ² = 0.003**		**σ² = 0.008**		**σ² = 0.010**	
		DM			s = -5.240	β = -0.09							s = 3.142					
	Fiber length	ADD													s = 3.698	*P* = 0.206		
		PSEU			s = -4.522	β = -0.19							s = -2.475					
		PTG			s = 3.458	β = 0.13					s = 1.483	*P* = 0.073			s = -4.593	*P* = 0.092	s = -1.393	*P* = 0.153
		CONST			s = 10.926	β = 0.23												
		Model	***P* = 0,004** **R² = 0,540**		*P* = 0,198 R² = 0,077		***P* = 0,040** **R² = 0,289**		*P* = 0,150 R² = 0,138		σ² = 0,003		**0,002**		σ² = 0,001		**0,002**	
		DM					s = 0,991	β = 0,09										
	PCSA	ADD									s = -2,104	*P* = 0,129	s = -2,408	*P* = 0,144	s = -1,736	*P* = 0,098	s = -1,985	*P* = 0,079
		PSEUDO					s = -1,311	β = -0,14					s = 1,724	*P* = 0,169			s = 1,361	*P* = 0,094
		PTGOID	s = -1,149	β = -0,15											s = 0,977	*P* = 0,083	s = 1,049	*P* = 0,222
		PTGDEI																
		Model	***P* = 0,018** **R² = 0,501**		*P* = 1		*P* = 0,07 R² = 0,226		***P* = 0,009** **R² = 0,506**		σ² = 0,002		0,002		σ² = 0,001		**0,002**	
		DM							s = 1,273	β = 0,07							s = 0,884	*P* = 0,167
SDh	Mass	ADD	s = -0,679	β = -0,08													s = -4,435	*P* = 0,023
		PSEUDO							s = -5,846	β = -0,28							s = 4,949	*P* = 0,010
		PTGOID							s = 5,671	β = 0,27								
		PTGDEI	s = -0,734	β = -0,08														
		Model	***P* = 0,010** **R² = 0,713**		*P* = 0,119 R² = 0,381		*P* = 0,182 R² = 0,192		*P* = 0,139 R² = 0,195		σ² = 0,003		**0,001**		σ² = 0,002		0,003	
		DM	s = -7,639	β = -0,25														
	Fiber length	ADD	s = -7,913	β = -0,32									s = -2,553	*P* = 0,078				
		PSEUDO	s = 5,820	β = 0,24														
		PTGOID	s = 3,225	β = 0,13									s = -2,852	*P* = 0,061				
		PTGDEI																